Science Advances
AAAS

Supplementary Materials for

Solvent-responsive covalent organic framework membranes for precise and tunable molecular sieving

Hao Yang *et al.*

Corresponding author: Dan Zhao, chezhao@nus.edu.sg

Sci. Adv. **10**, eads0260 (2024)
DOI: 10.1126/sciadv.ads0260

This PDF file includes:

Supplementary Materials and Methods
Supplementary Text
Figs. S1 to S43
Tables S1 and S2
References

Chemicals and materials

Polyvinylidene fluoride (PVDF) substrate (molecular weight cut-off of 100,000 Da) was purchased from Beijing Haicheng Shijie Co Ltd. Ethanol (>99.8%), *N,N*-dimethylformamide (DMF, >99.5%), dichloromethane (DCM, >99.5%), methanol (>99.5%), tetrahydrofuran (THF, >99.5%), ethyl acetate (>99.5%), carbon tetrachloride (CTC, >99.5%), cyclohexane (>99%), toluene (>99.5%), *n*-heptane (>99.5%), *n*-hexane (>99.5%), *iso*-propanol (>99.5%), chloroform (>99.5%), and acetone (>99.5%) were obtained from Avantor Performance Materials Inc. Dopamine (97%) and tris(hydroxymethyl)aminomethane-hydrochloride (tris-HCl, 95%) were purchased from Alfa Aesar. 2,4,6-Tris(4-aminophenyl)-1,3,5-triazine (TAPT, 98%), mesitylene (>99.5%), and tris(4-aminophenyl)amine (TAPA, 99%) were purchased from Tee Hai Chem Pte Ltd. 1,3,5-Triformylphloroglucinol (Tp, 98%) and 1,6-diaminopyrene (DAP, 98%) were purchased from Yanshen Technology Co Ltd. Congo red (>95%), acid fuchsin (>95%), methyl blue (>95%), methyl orange (>95%), acid blue (>95%), $Ir[dF(CF_3)ppy]_2(dtbpy))PF_6$ (>99%), Hoveyda-Grubbs Catalyst® M720 (>95%), and tris(2,2'-bipyridine)ruthenium(II) hexafluorophosphate (>98%) were purchased from Sigma-Aldrich. Curcumin (>95%), tetracycline (>95%), and chlorophyll (>95%) were purchased from Tokyo Chemical Industry (TCI) Co., Ltd. All the purchased materials were directly used without further purification. The deionized water was used throughout the experiments.

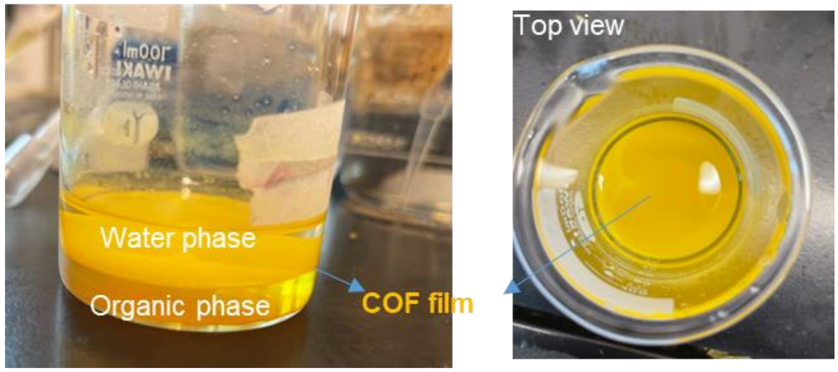

Fig. S1. Optical images of the synthesized COF Tp-TAPT film at the interface between water phase and organic phase.

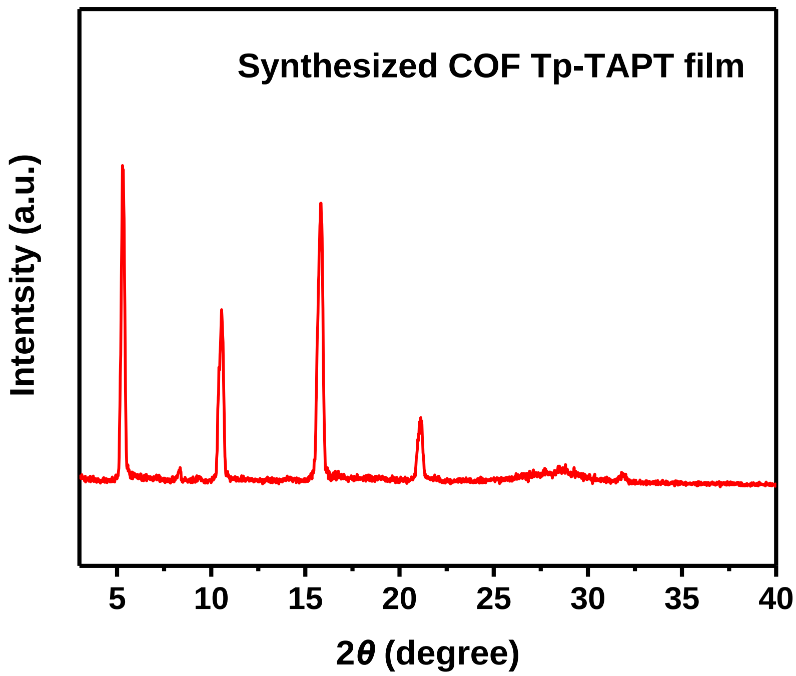

Fig. S2. Powder X-ray diffraction (PXRD) pattern of the synthesized COF Tp-TAPT film.

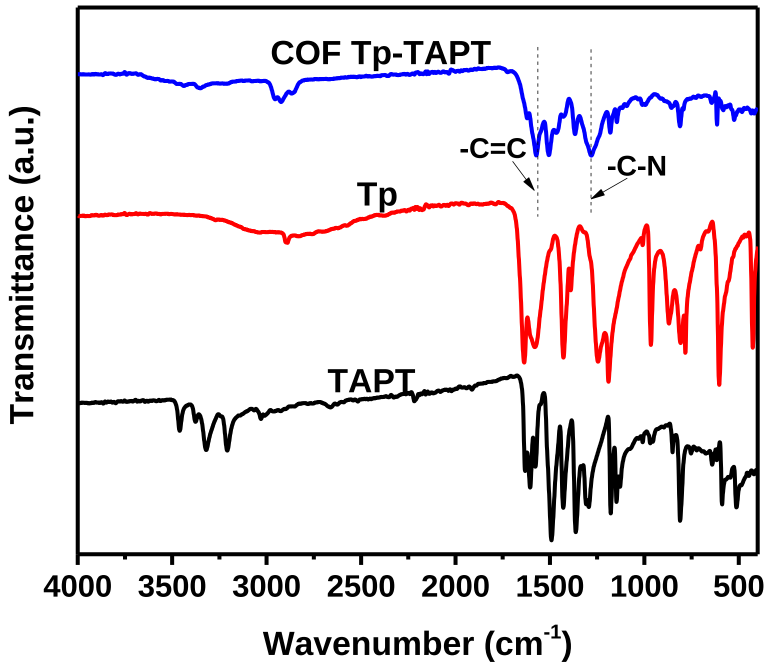

Fig. S3. FTIR spectra of Tp monomer, TAPT monomer, and COF Tp-TAPT film.

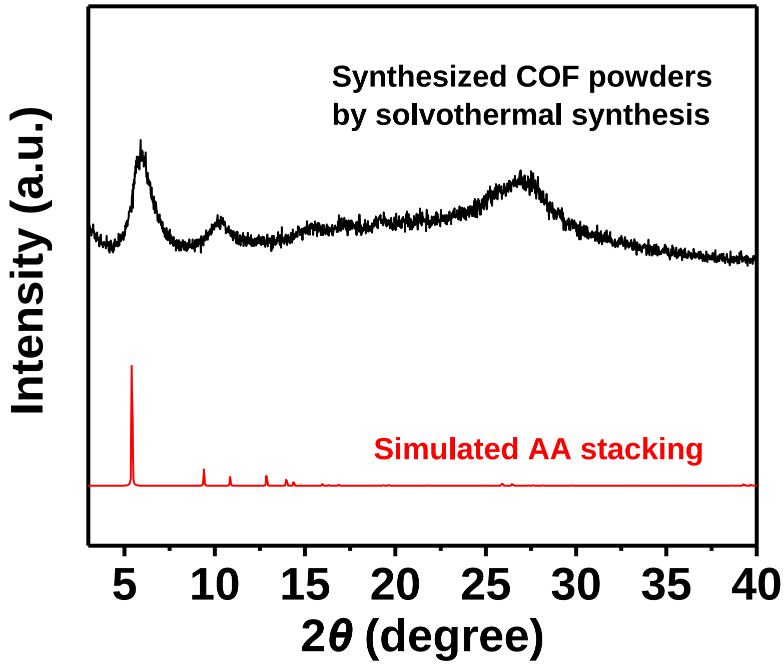

Fig. S4. PXRD patterns of the synthesized COF TpTAPT powders by solvothermal synthesis with simulated AA stacking structures.

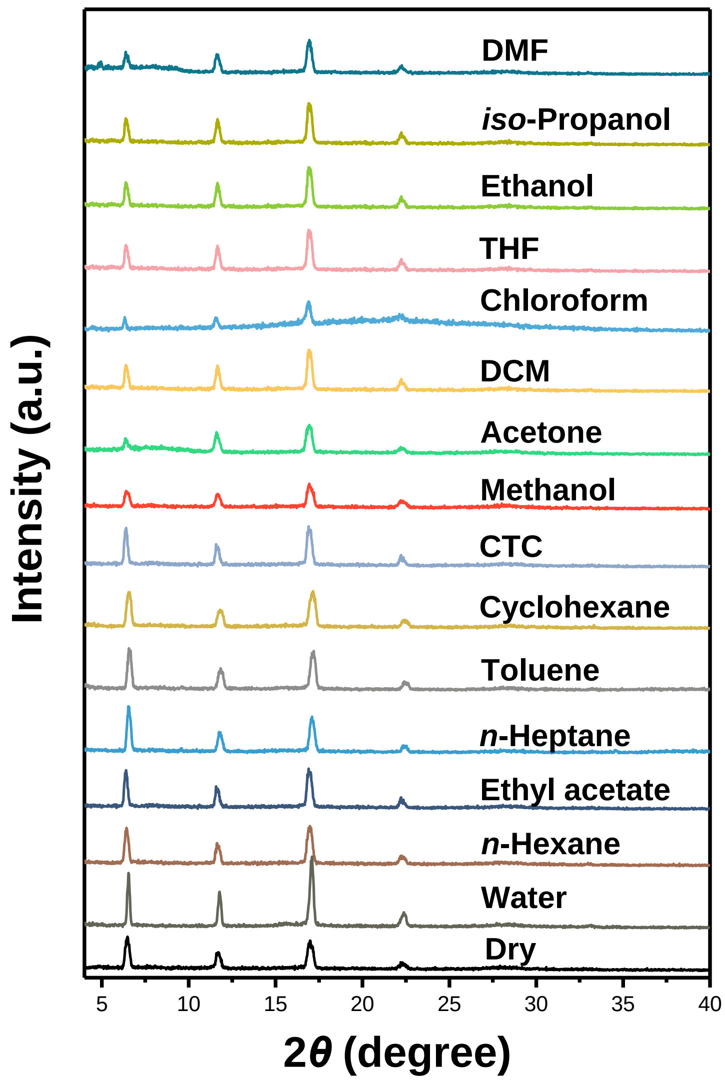

Fig. S5. PXRD patterns of the COF Tp-TAPT films solvated by various solvents.

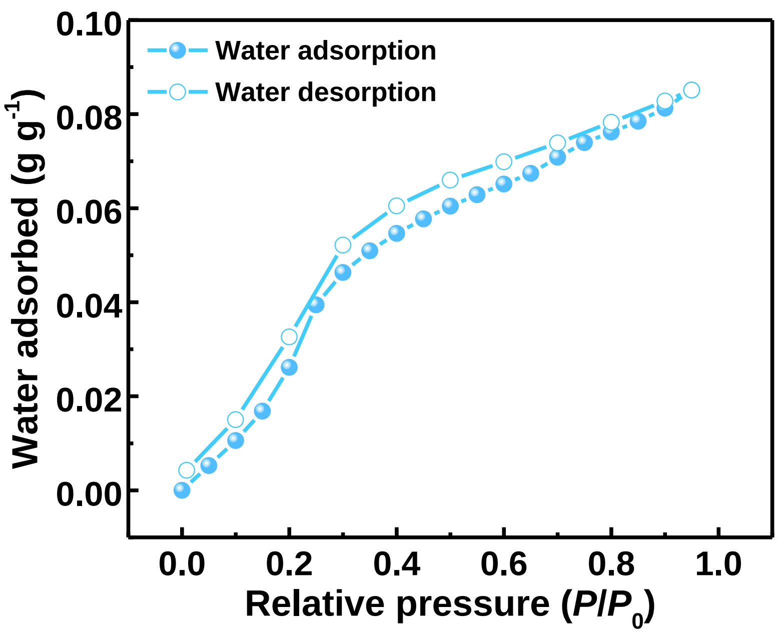

Fig. S6. Water vapor adsorption-desorption isotherms of COF Tp-TAPT measured at 298 K.

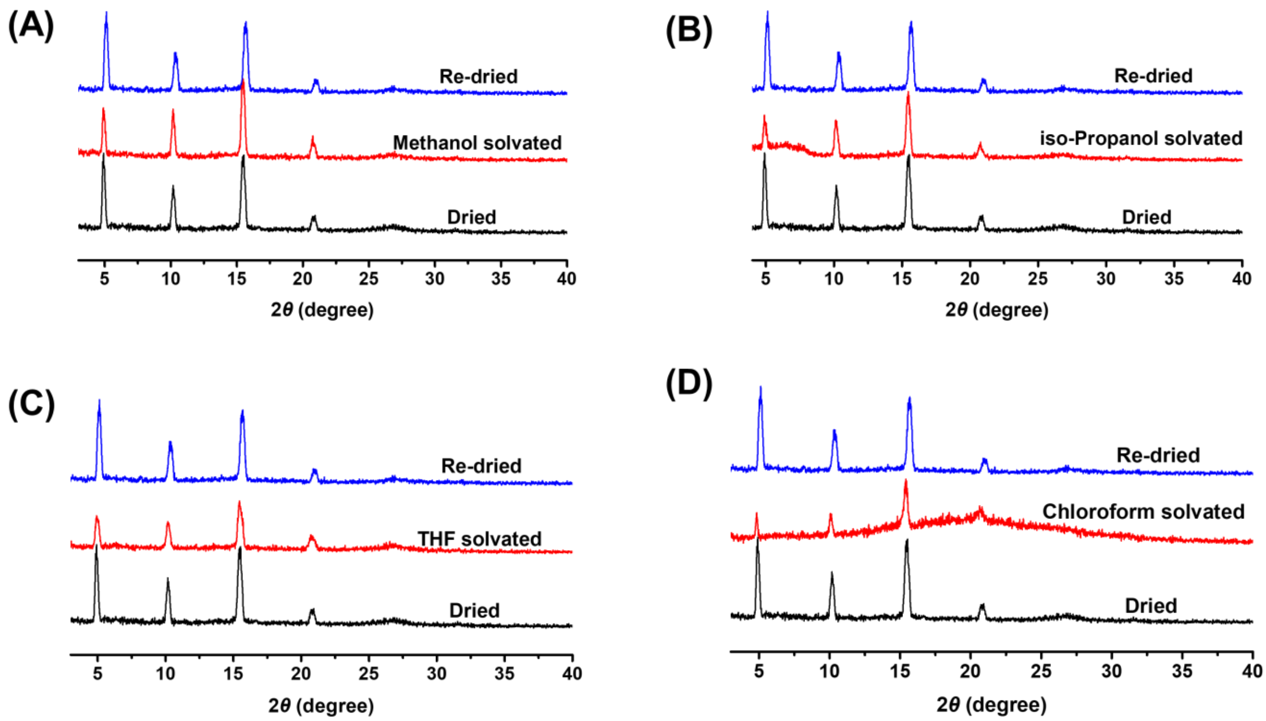

Fig. S7. PXRD patterns of sequential dried−solvated−dried COF Tp-TAPT film in (A) methanol, (B) *iso*-propanol, (C) THF, and (D) chloroform.

Table S1. Viscosity, molar volume, solvent molar diameter, and Hansen solubility parameter of the solvents used in this study.

Solvent	Viscosity (mPa s)[a]	Molar volume (V_m, cm^3 mol^{-1})[b]	d_m (nm)[c]	Hansen solubility parameter ($MPa^{1/2}$)[d]				Remarks
				δ_d	δ_p	δ_h	$\delta_0 = (\delta_d^2 + \delta_p^2 + \delta_h^2)^{1/2}$	
***n*-Hexane**	0.30	130.5	0.72	14.9	0.0	0.0	14.9	Solvents that **cannot** trigger interlayer shifting
Cyclohexane	0.90	105.5	0.69	16.8	0.0	0.2	16.8	
***n*-Heptane**	0.40	146.5	0.77	15.3	0.0	0.0	15.3	
Toluene	0.56	106.3	0.70	18.0	1.4	2.0	18.2	
Ethyl acetate	0.42	97.8	0.68	15.8	5.3	7.2	18.2	
CTC	0.97	96.5	0.67	17.8	0.0	0.6	17.8	
Water	0.89	18.1	0.39	15.5	16.0	42.3	47.8	
Acetone	0.31	73.9	0.62	15.5	10.4	7.0	19.9	Solvents that **can** trigger interlayer shifting
THF	0.48	74.0	0.62	16.8	5.7	8.0	19.5	
DCM	0.44	64.0	0.59	17.8	6.2	6.0	19.8	
Chloroform	0.54	80.5	0.63	17.8	3.1	5.7	18.9	
DMF	0.82	77.0	0.63	17.4	13.7	11.3	24.9	
Methanol	0.55	40.7	0.51	15.1	12.3	22.3	29.6	
Ethanol	1.07	58.7	0.57	15.8	8.8	19.4	26.5	
***iso*-Propanol**	2.04	75.1	0.62	15.8	6.1	16.4	23.6	

[a] Viscosity is at 25 °C (*61*).

[b] Molar volume (V_m) data were taken from ref (*6, 62*).

[c] Molar diameter (d_m) was calculated from ref (*6*) using V_m of the solvent molecules with the equation: $d_m = 2 \times (3V_m/4\pi N_A)^{1/3}$, where N_A is Avogadro's number.

[d] δ_d is solubility parameter contributed by dispersion forces, δ_p is solubility parameter contributed by dipole forces, δ_h is solubility parameter contributed by hydrogen bonding (or contributed by donoracceptor interactions), and δ_0 is total solubility parameter (*63*).

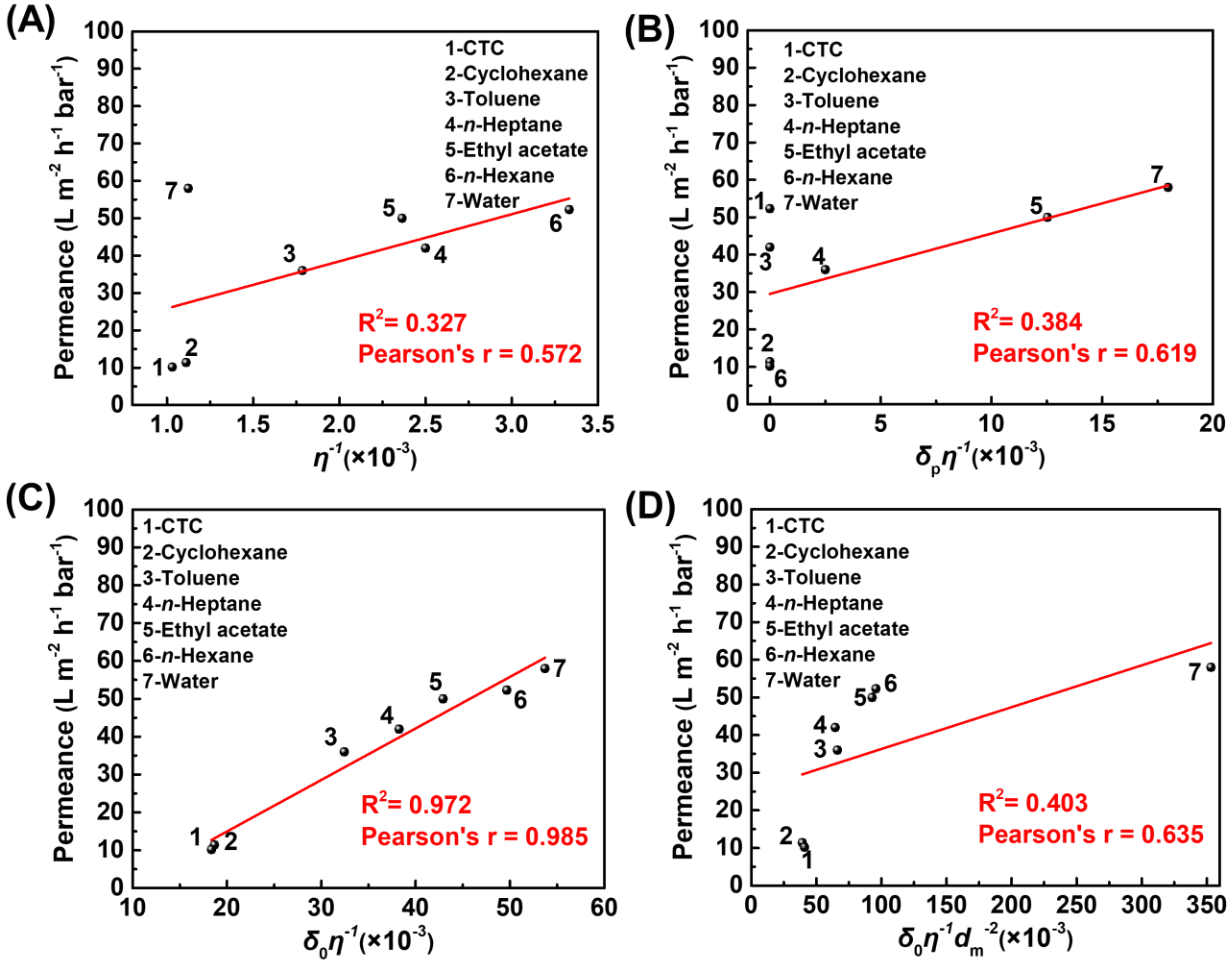

Fig. S8. Analysis of solvent transport through COF Tp-TAPT membrane in nonpolar organic solvents, low-polarity organic solvents, and water. (A) Plot and fitting of solvent permeance against solvent viscosity. (B) Plot and fitting of solvent permeance against the combined solvent property (solubility parameter due to dipole forces and viscosity). (C) Plot and fitting of solvent permeance against the combined solvent property (total solubility parameter and viscosity). (D) Plot and fitting of solvent permeance against the combined solvent property (total solubility parameter, viscosity, and molar diameter).

Note: According to figure (C), solvent permeance follows the equation:

$$J \propto K_{HP}\ \delta_0\ \eta^{-1}\ \Delta P$$

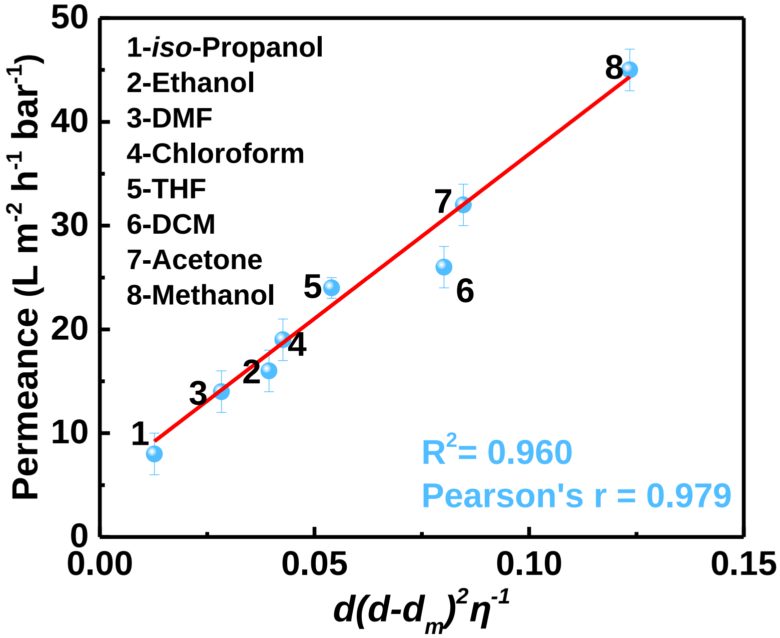

Fig. S9. Plot and fitting of solvent permeance against the model parameter combining solvent viscosity, membrane pore size, and kinetic diameter of solvent.

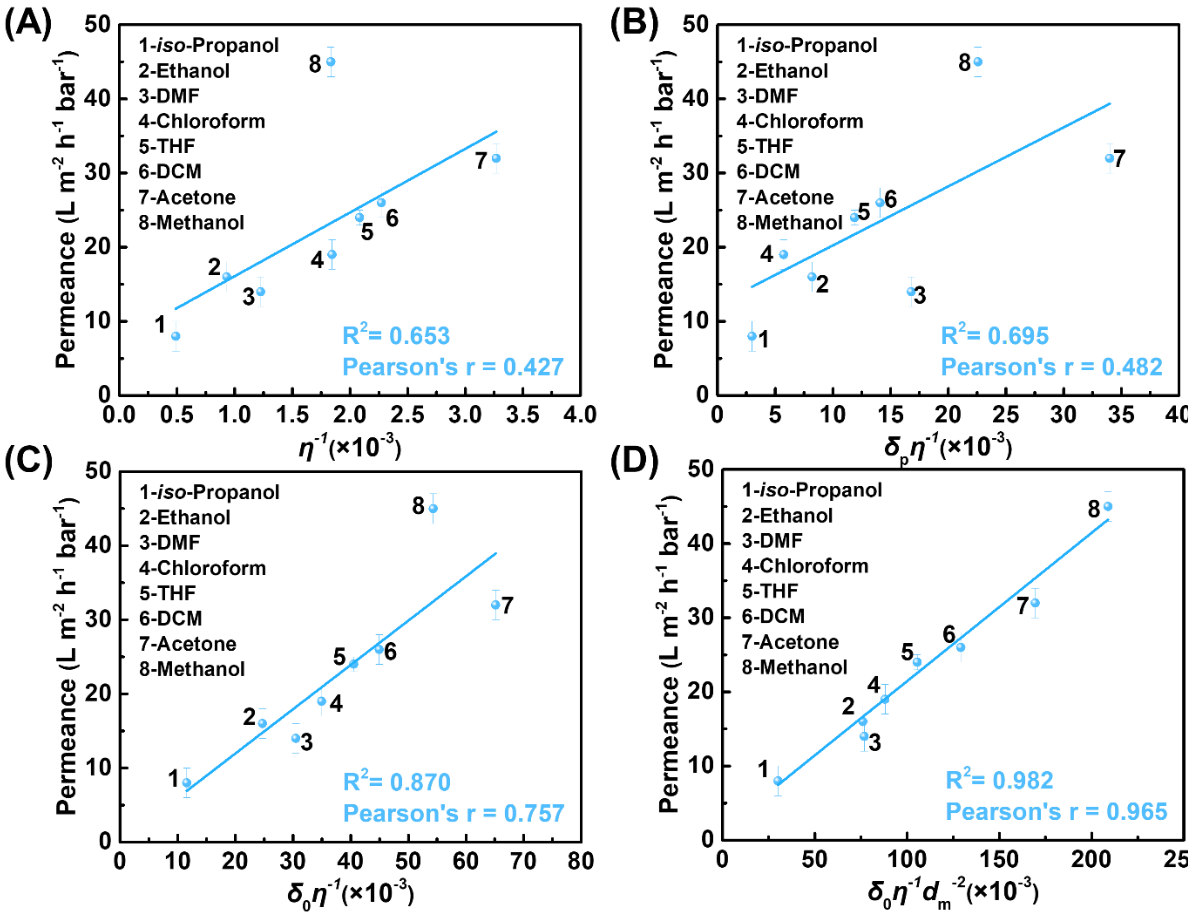

Fig. S10. Analysis of solvent transport through COF Tp-TAPT membrane in polar organic solvents. (A) Plot and fitting of solvent permeance against solvent viscosity. (B) Plot and fitting of solvent permeance against the combined solvent property (solubility parameter due to dipole forces and viscosity). (C) Plot and fitting of solvent permeance against the combined solvent property (total solubility parameter and viscosity). (D) Plot and fitting of solvent permeance against the combined solvent property (total solubility parameter, viscosity, and molar diameter).

Note: According to figure (D), solvent permeance follows the equation:

$$J \propto K_{HP}\ \delta_0\ \eta^{-1}\ d_m^{-2} \Delta P$$

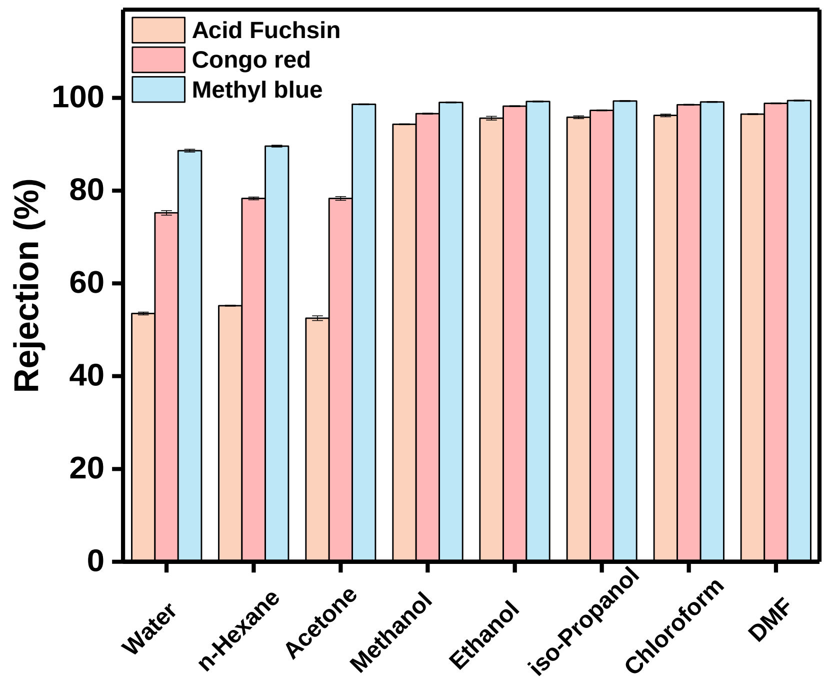

Fig. S11. Dye rejection performance of COF Tp-TAPT membrane in different solvents.

Note: The feed concentration is 50 ppm, and the operation pressure is 2 bar.

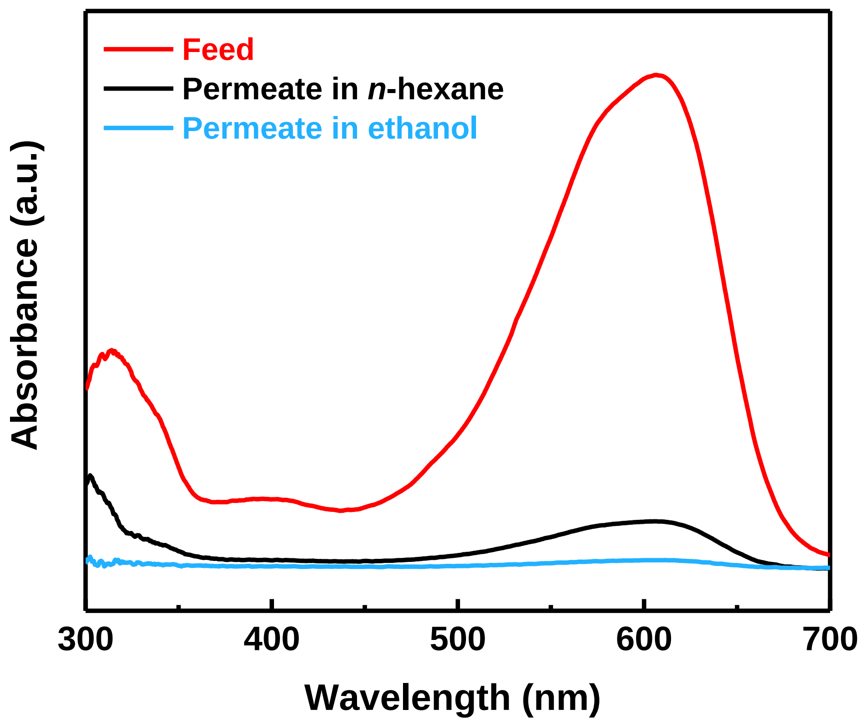

Fig. S12. UV-Vis spectra of the feed, permeate in *n*-hexane, and permeate in ethanol for rejecting methyl blue by COF Tp-TAPT membrane.

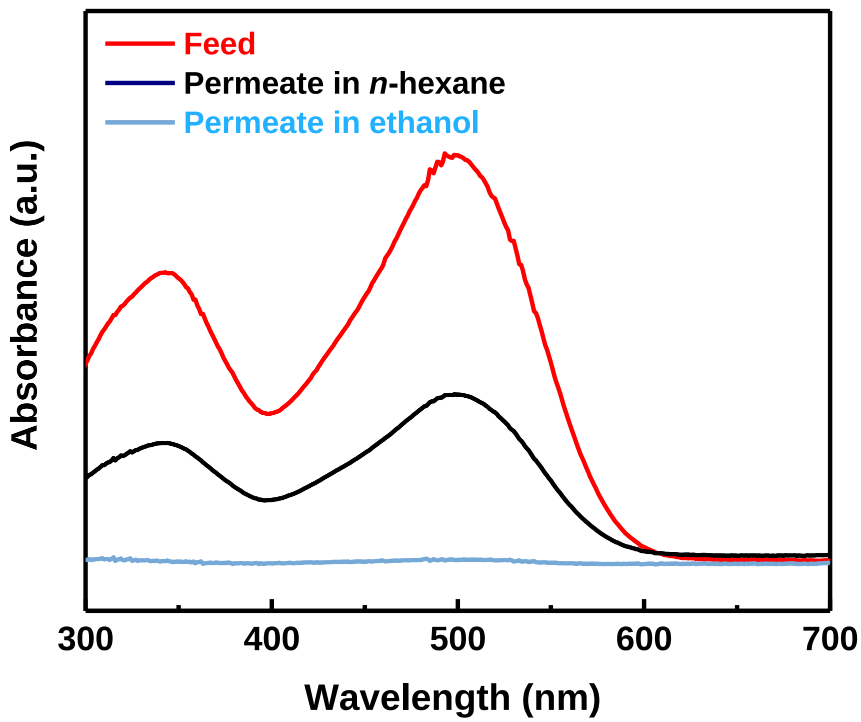

Fig. S13. UV-Vis spectra of the feed, permeate in *n*-hexane, and permeate in ethanol for rejecting Congo red by COF Tp-TAPT membrane.

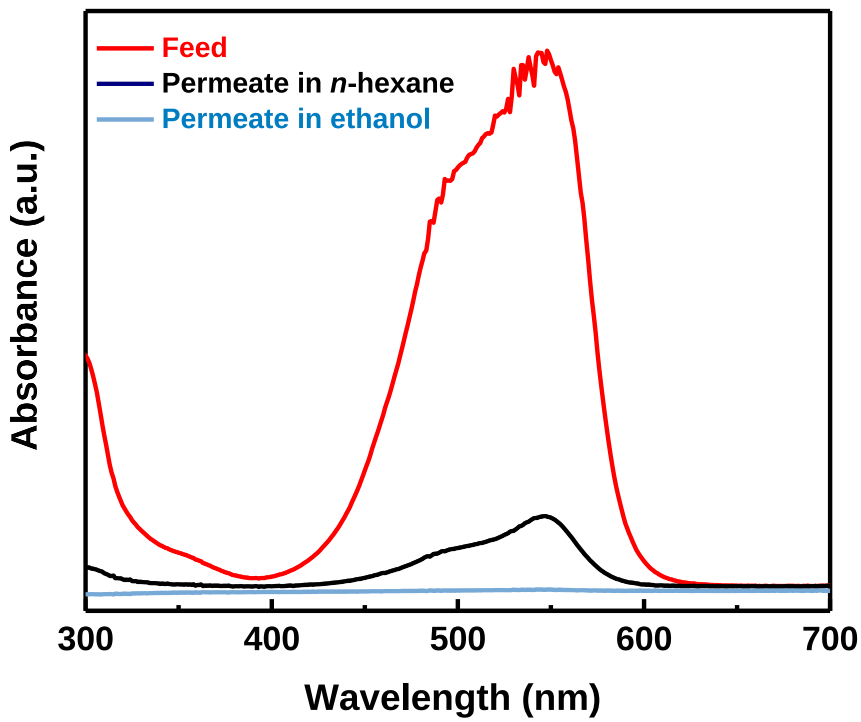

Fig. S14. UV-Vis spectra of the feed, permeate in *n*-hexane, and permeate in ethanol for rejecting acid fuchsin by COF Tp-TAPT membrane.

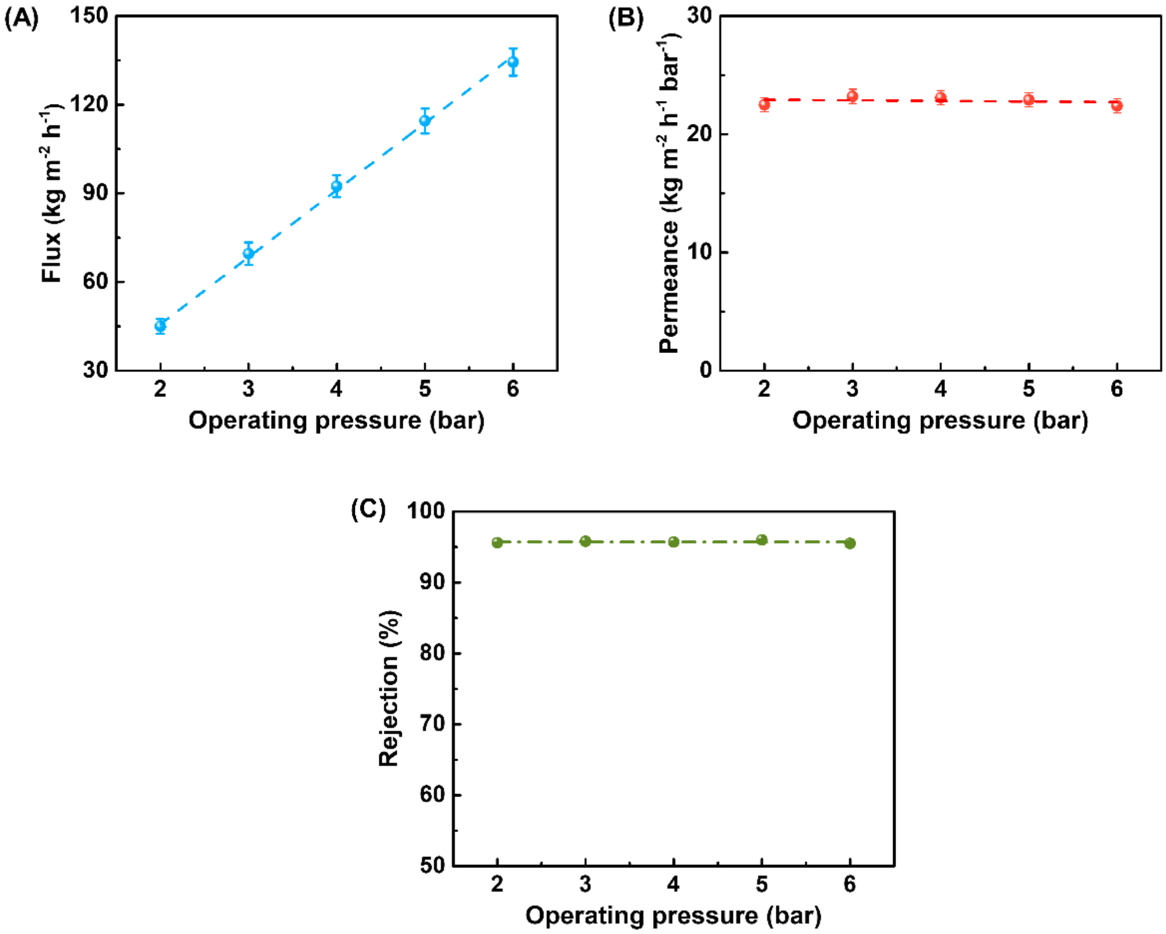

Fig. S15. (A) Flux, (B) permeance, and (C) rejection as a function of operating pressure for rejecting acid fuchsin in ethanol by COF Tp-TAPT membrane.

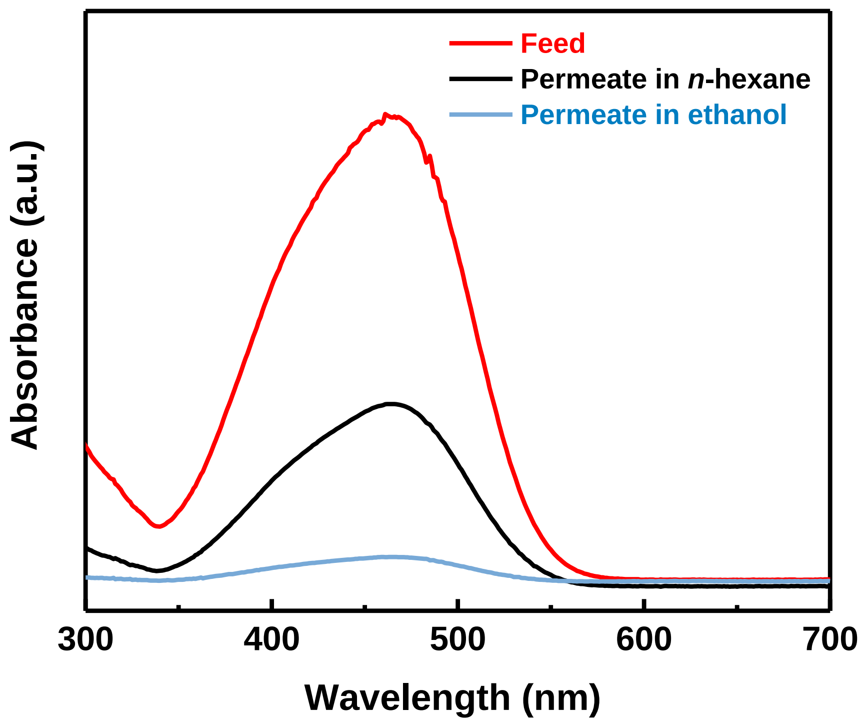

Fig. S16. UV-Vis spectra of the feed, permeate in *n*-hexane, and permeate in ethanol for rejecting methyl orange by COF Tp-TAPT membrane.

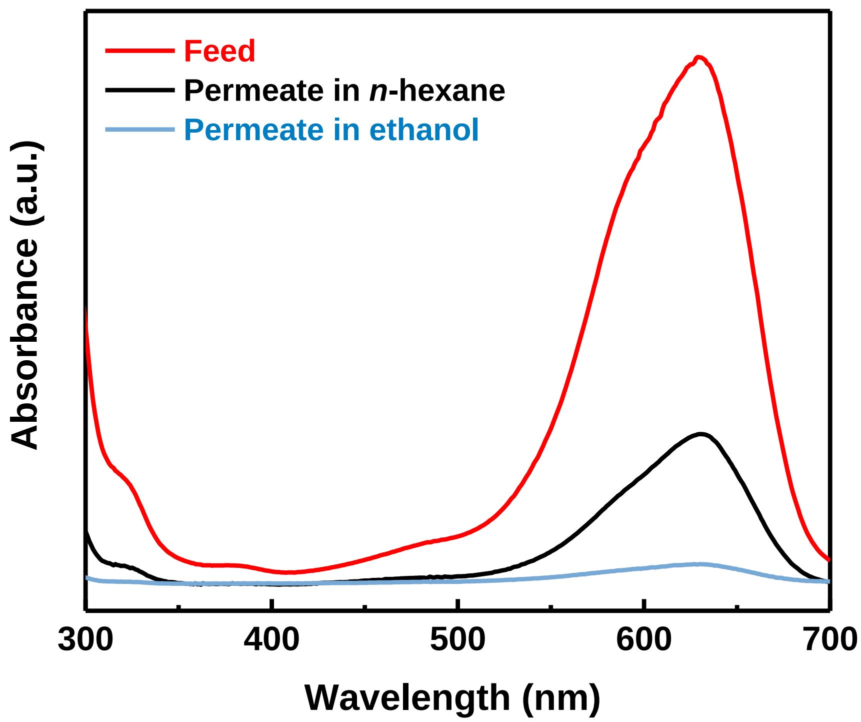

Fig. S17. UV-Vis spectra of the feed, permeate in *n*-hexane, and permeate in ethanol for rejecting acid blue by COF Tp-TAPT membrane.

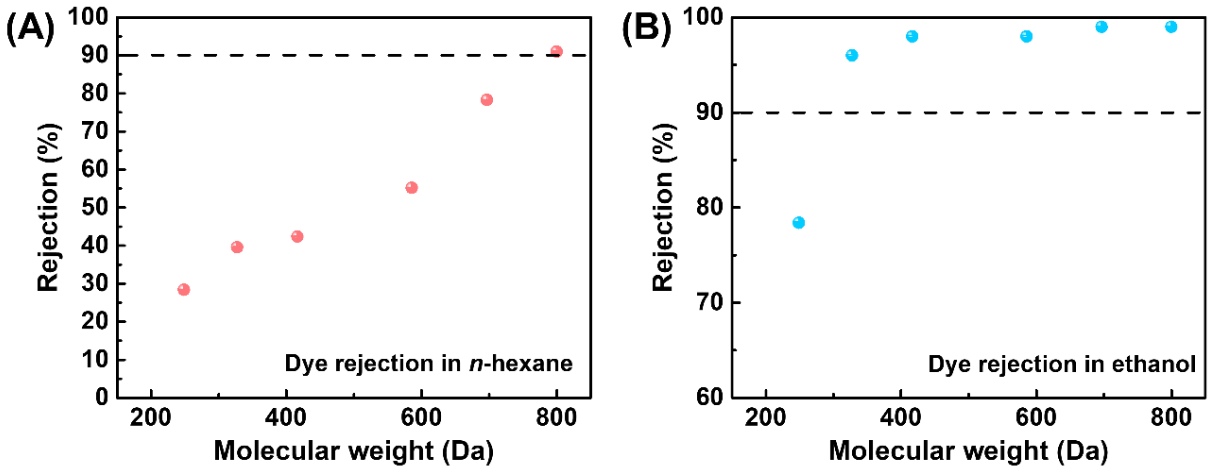

Fig. S18. Dye rejection curves in (A) *n*-hexane and (B) ethanol.

Note: The feed concentration is 50 ppm, and the operation pressure is 2 bar.

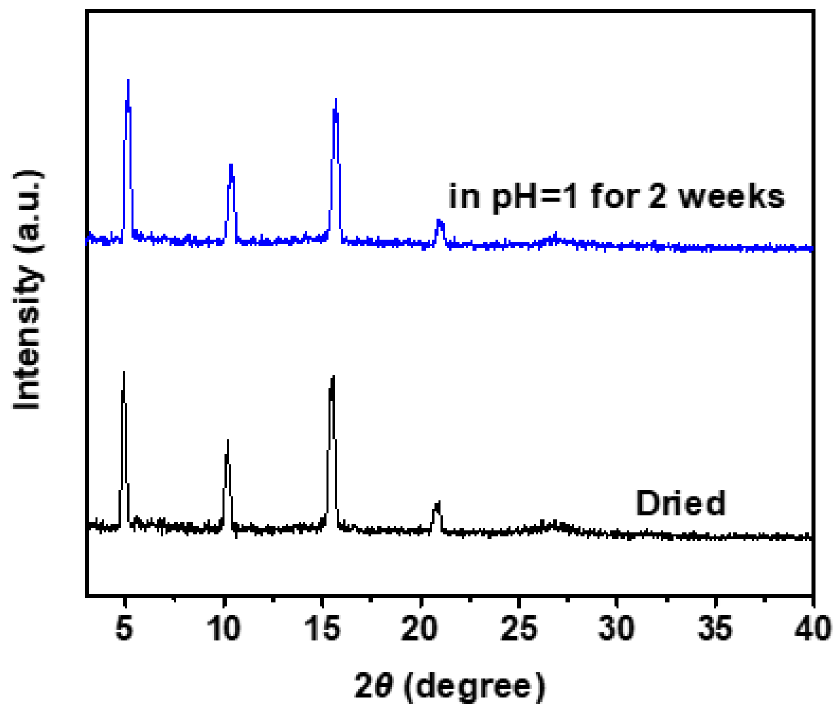

Fig. S19. The PXRD patterns of COF Tp-TAPT film soaked in pH=1 aqueous solution for 2 weeks.

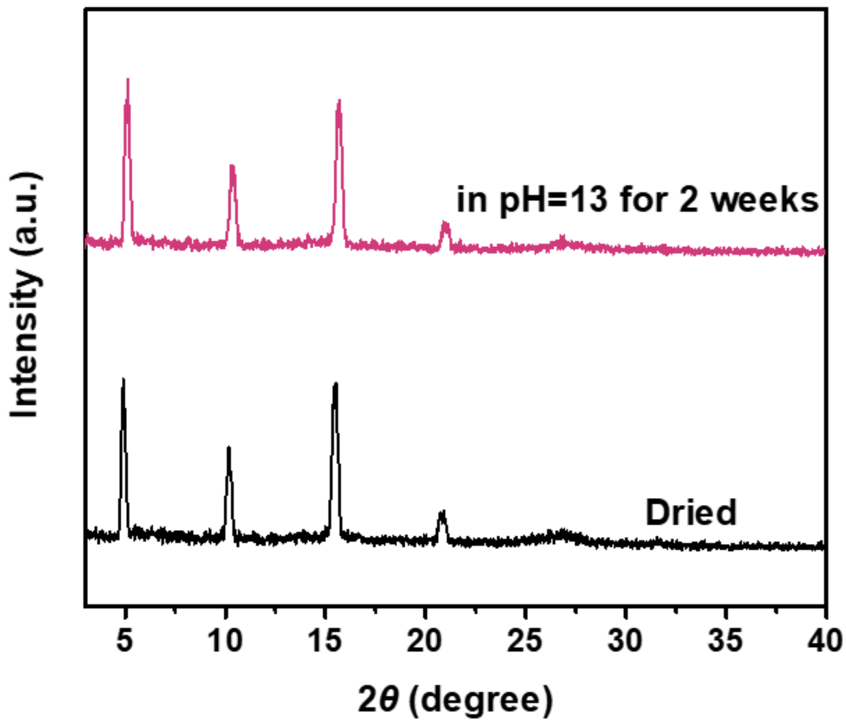

Fig. S20. The PXRD patterns of COF Tp-TAPT film soaked in pH=13 aqueous solution for 2 weeks.

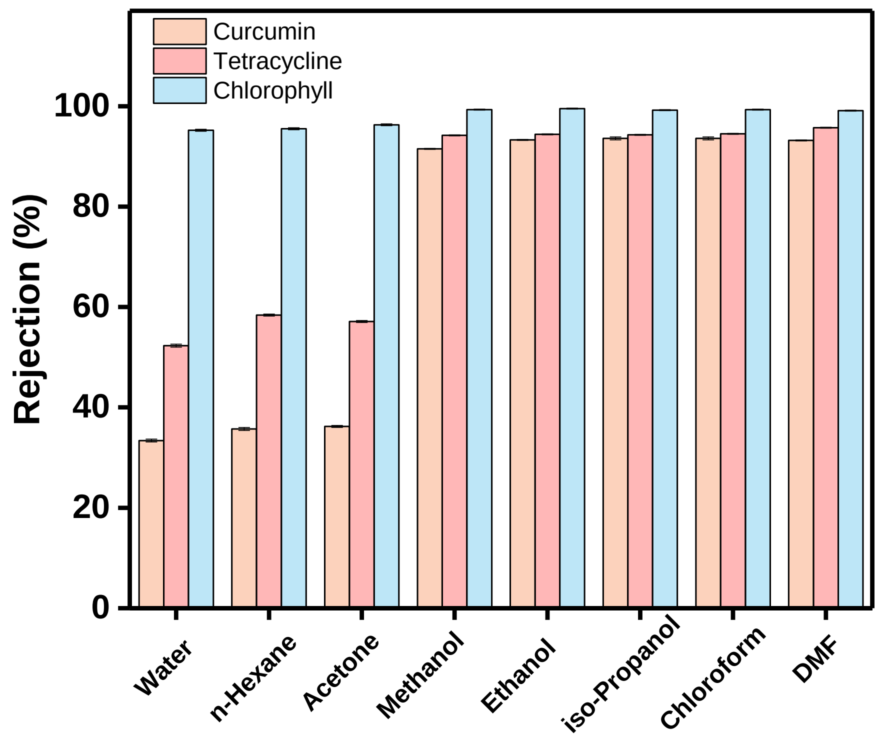

Fig. S21. Separation performance of COF TpTAPT membranes for rejecting APIs in different organic solvents.

Note: The feed concentration is 50 ppm, and the operation pressure is 2 bar.

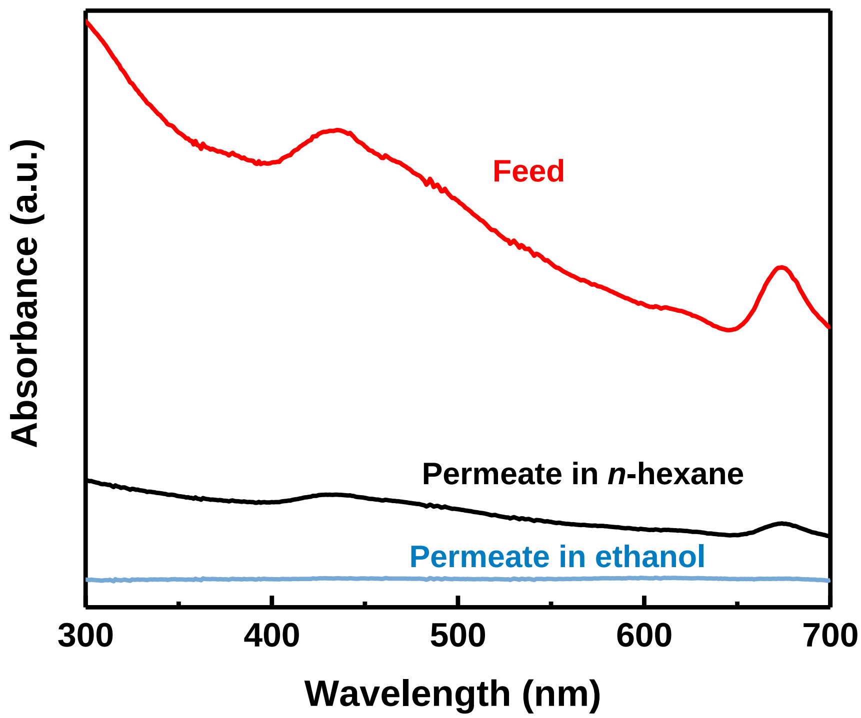

Fig. S22. UV-Vis spectra of the feed, permeate in *n*-hexane, and permeate in ethanol for rejecting chlorophyll by COF Tp-TAPT membrane.

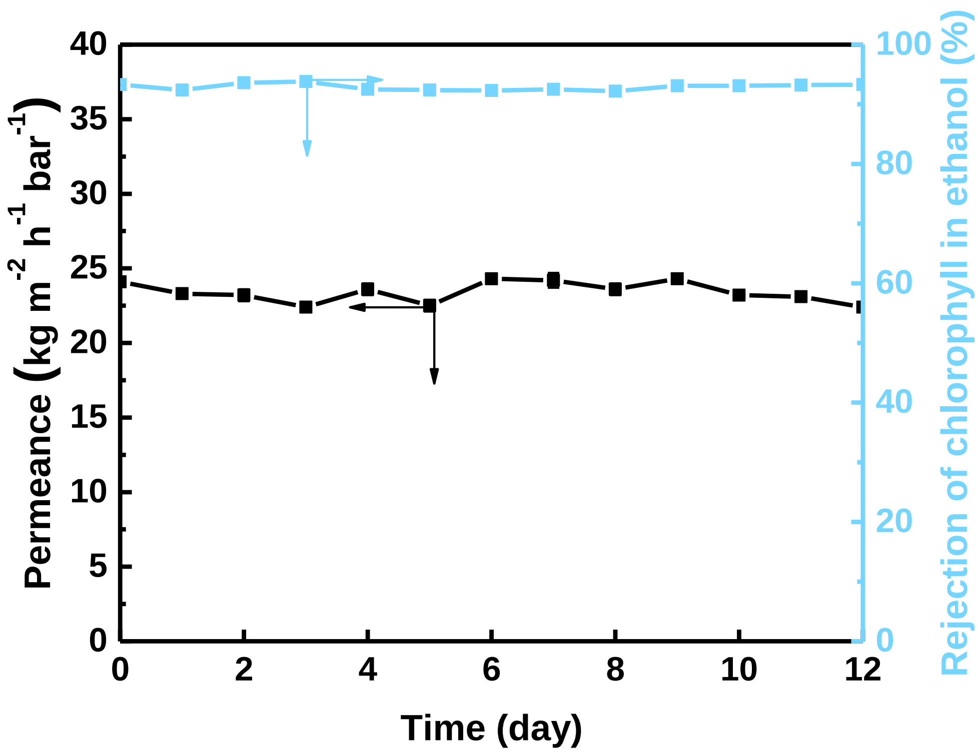

Fig. S23. Long-term separation performance of COF Tp-TAPT membrane for chlorophyll rejection in ethanol.

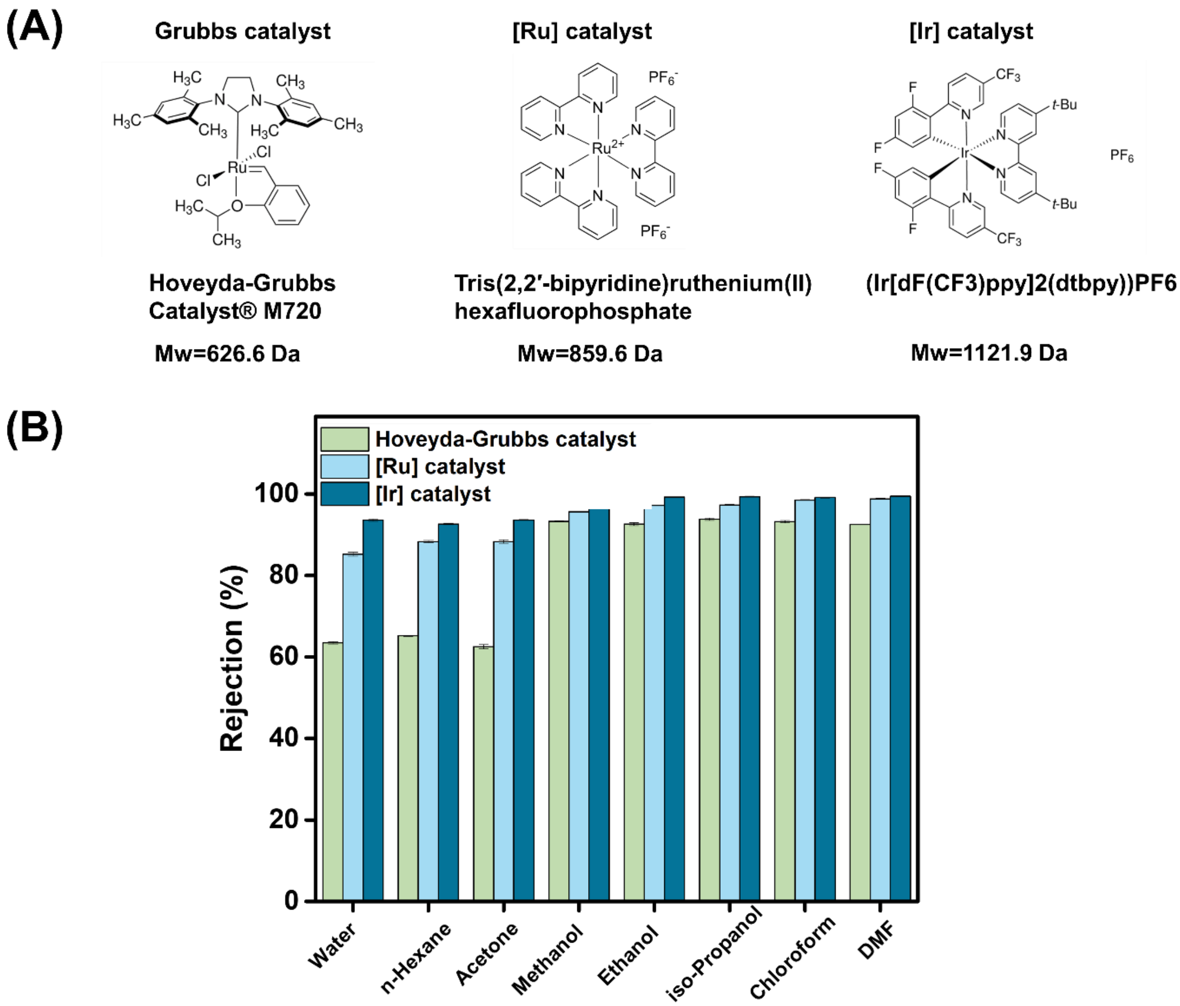

Fig. S24. (A) Chemical structures of Grubbs catalyst, [Ru] catalyst, and [Ir] catalyst. (B) Separation performance of COF TpTAPT membranes for rejecting the three homogeneous catalysts in different organic solvents.

Note: The feed concentration is 50 ppm, and the operation pressure is 3 bar.

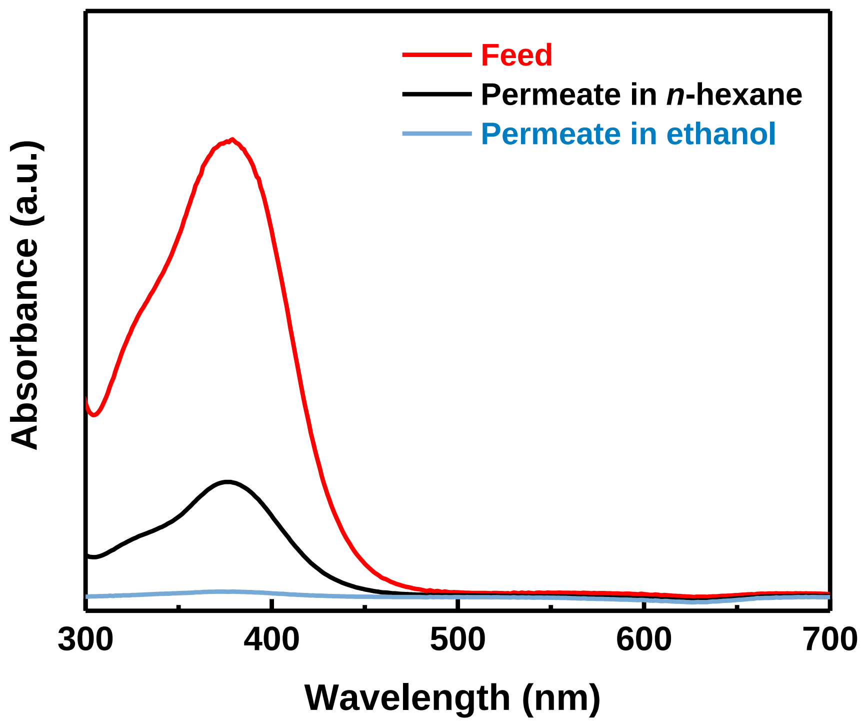

Fig. S25. UV-Vis spectra of the feed, permeate in *n*-hexane, and permeate in ethanol for rejecting Grubbs catalyst by COF Tp-TAPT membrane.

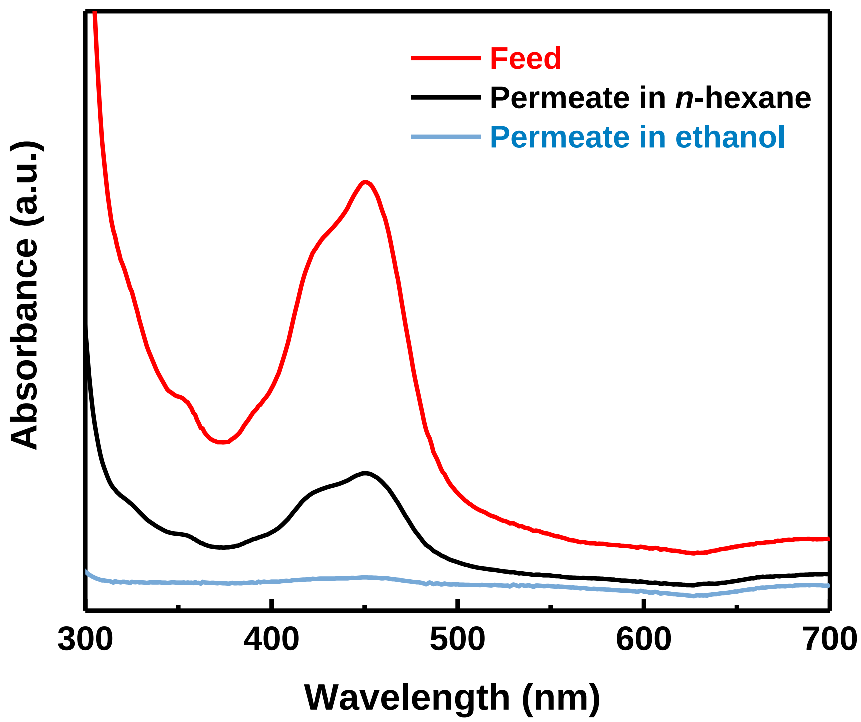

Fig. S26. UV-Vis spectra of the feed, permeate in *n*-hexane, and permeate in ethanol for rejecting [Ru] catalyst by COF Tp-TAPT membrane.

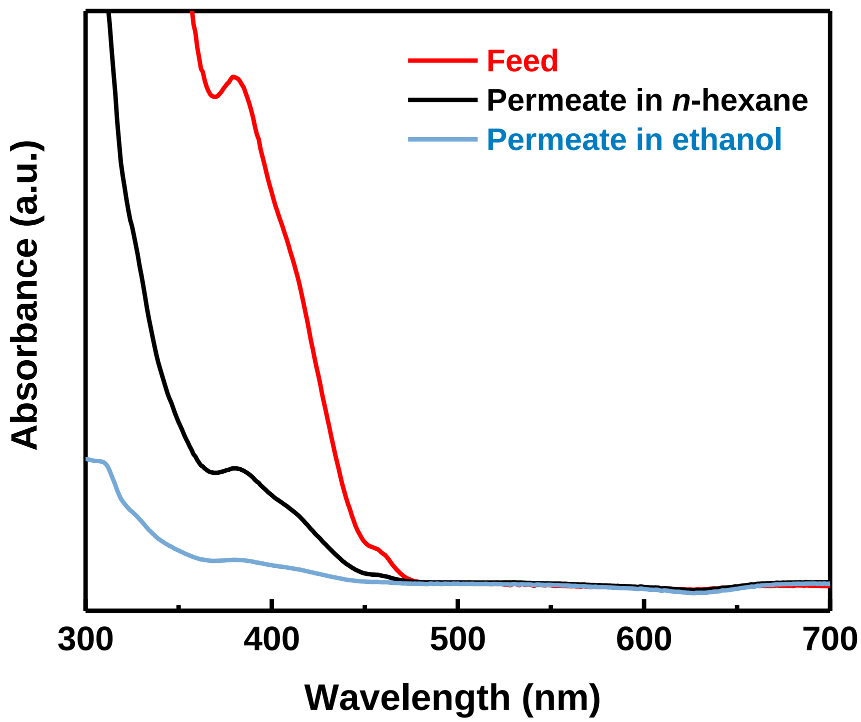

Fig. S27. UV-Vis spectra of the feed, permeate in *n*-hexane, and permeate in ethanol for rejecting [Ir] catalyst by COF Tp-TAPT membrane.

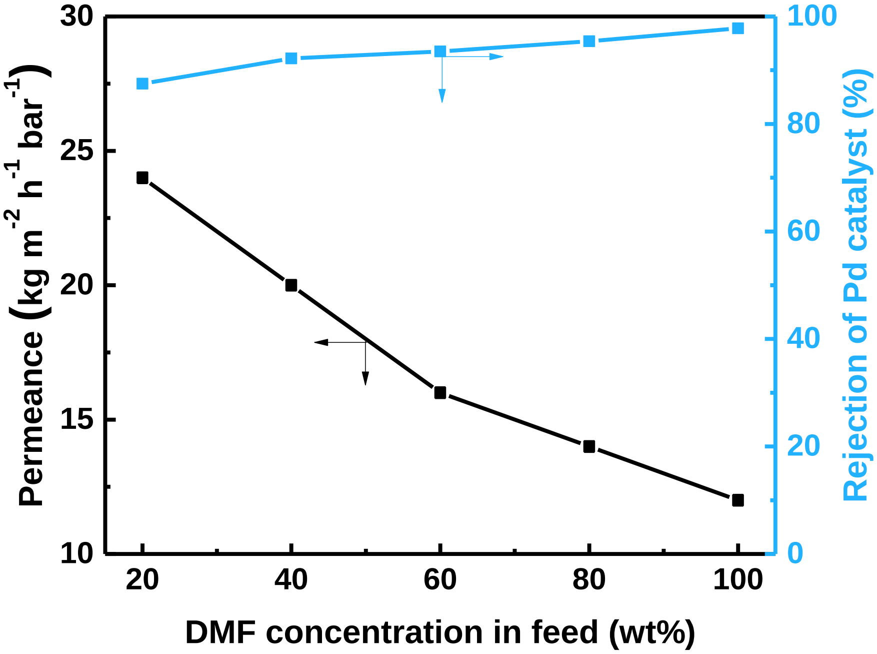

Fig. S28. Rejection of $Pd(OAc)_2PPh_3$ catalyst in DMF/ethanol mixed solvents by COF Tp-TAPT membrane.

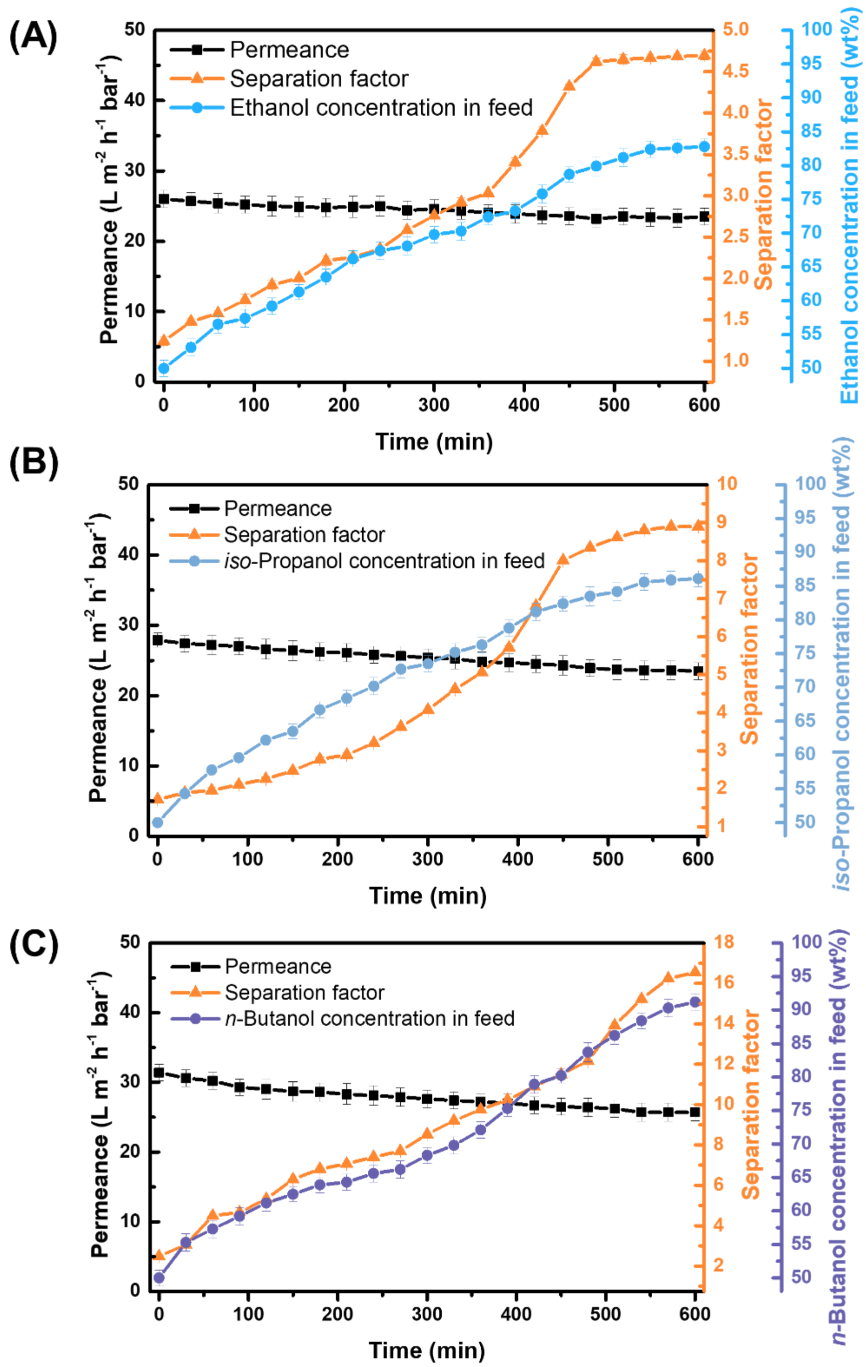

Fig. S29. Organic solvent reverse osmosis (OSRO) performance of the COF Tp-TAPT membrane for dehydration of (A) ethanol/water, (B) *iso*-propanol/water, and (C) *n*-butanol/water.

Note: The feed concentration is 50/50 wt% (water/alcohol). The operation pressure is 5 bar.

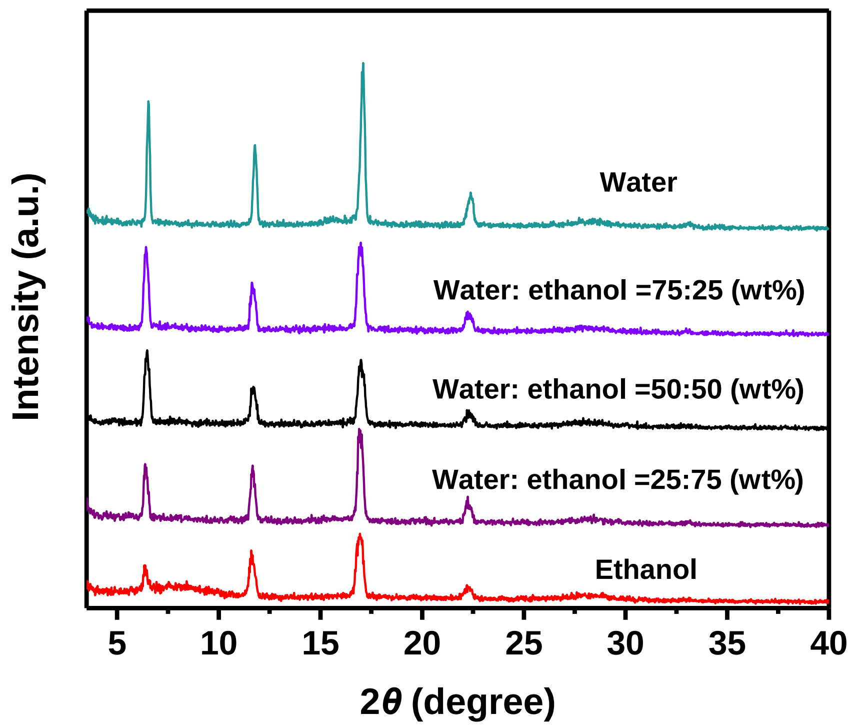

Fig. S30. PXRD patterns of the COF Tp-TAPT films in mixed solvents with different ethanol concentrations.

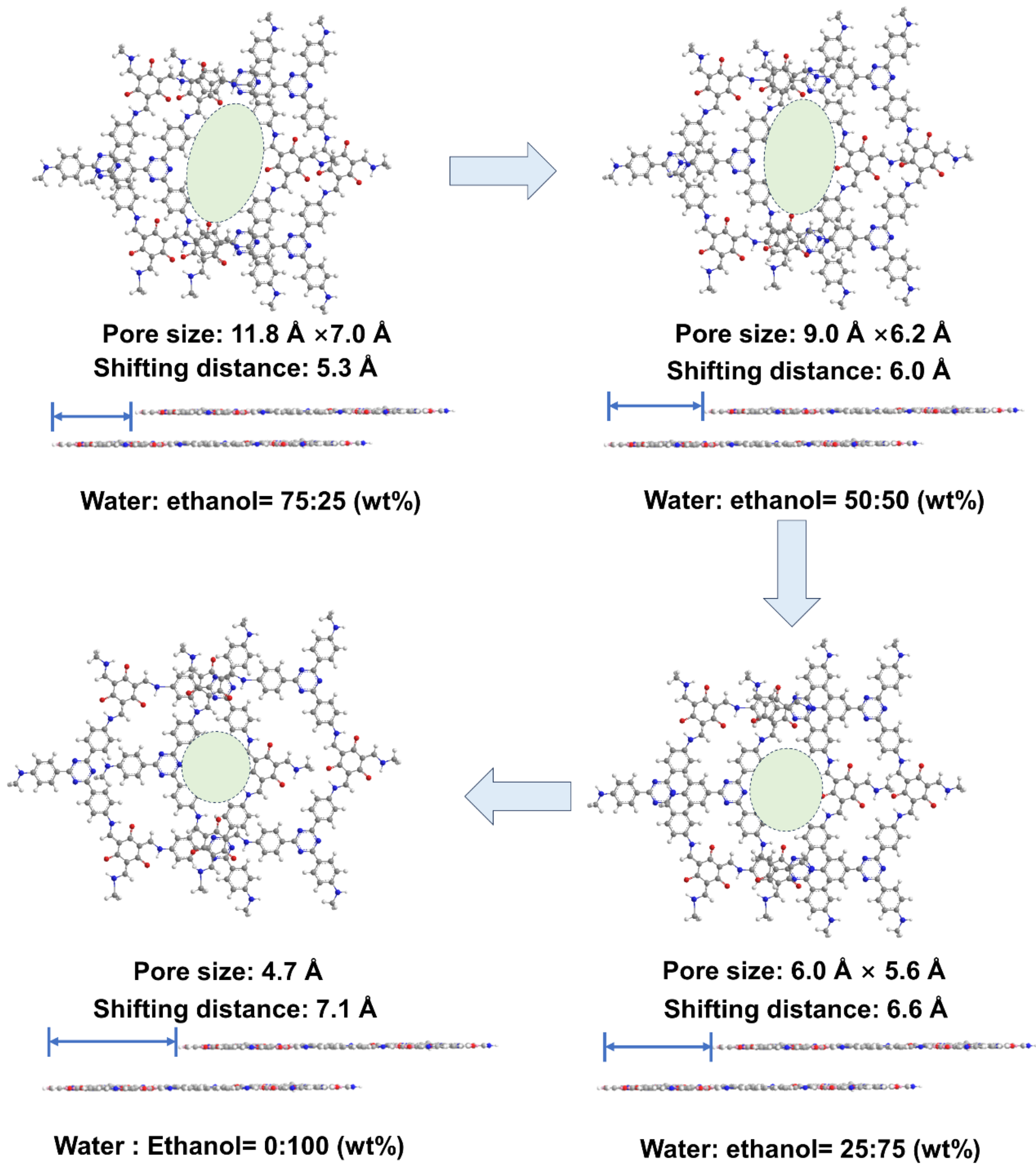

Fig. S31. Dynamic changes of the COF structure during the OSRO separation process by MD simulations.

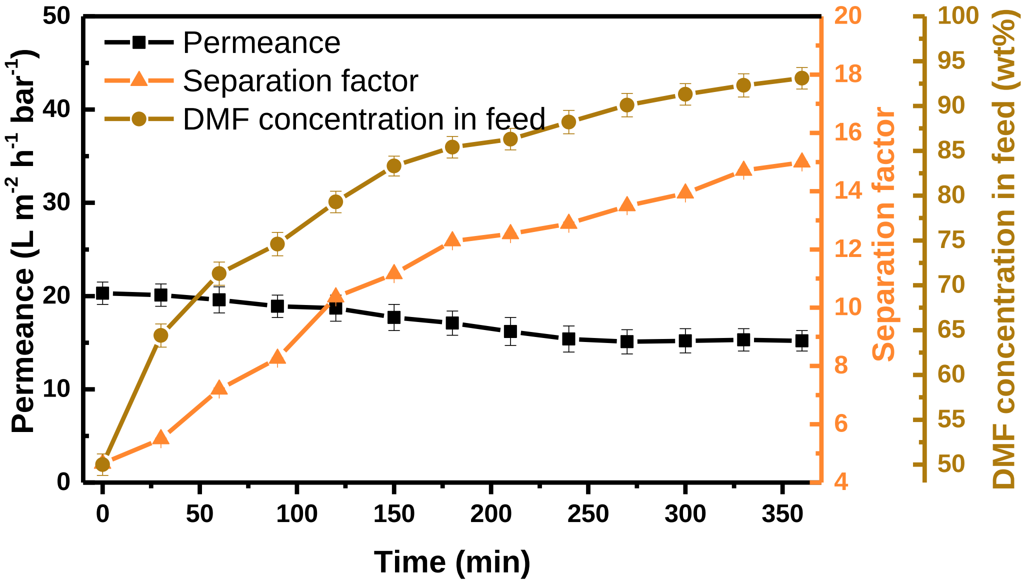

Fig. S32. DMF dehydration performance of the COF Tp-TAPT membrane by OSRO.

Note: The feed concentration is 50/50 wt% (water/DMF). The operation pressure is 5 bar.

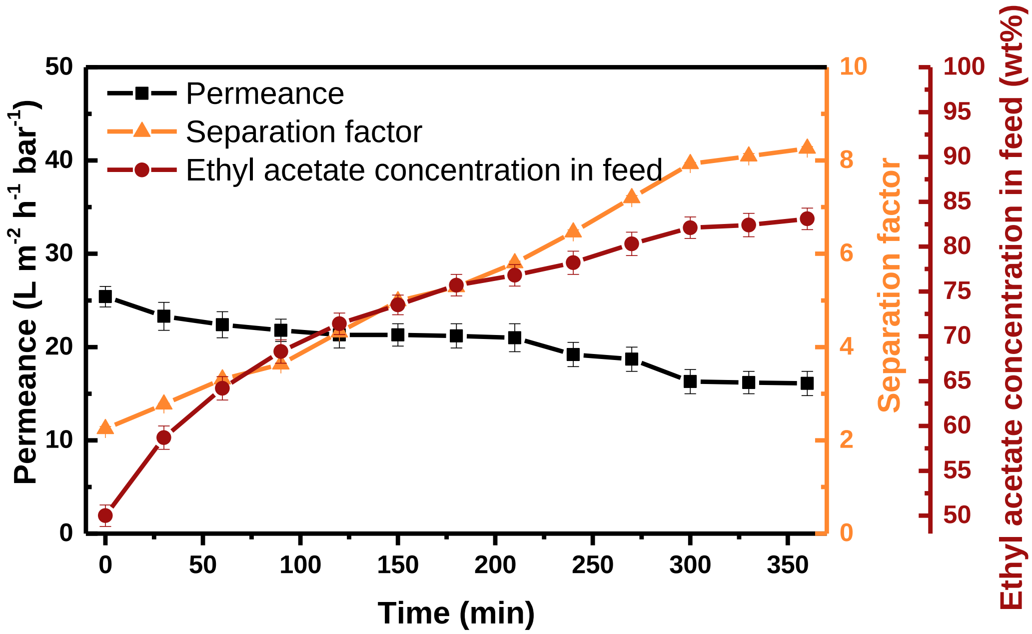

Fig. S33. Ethyl acetate dehydration performance of the COF Tp-TAPT membrane by OSRO.

Note: The feed concentration is 50/50 wt% (water/ethyl acetate). The operation pressure is 5 bar.

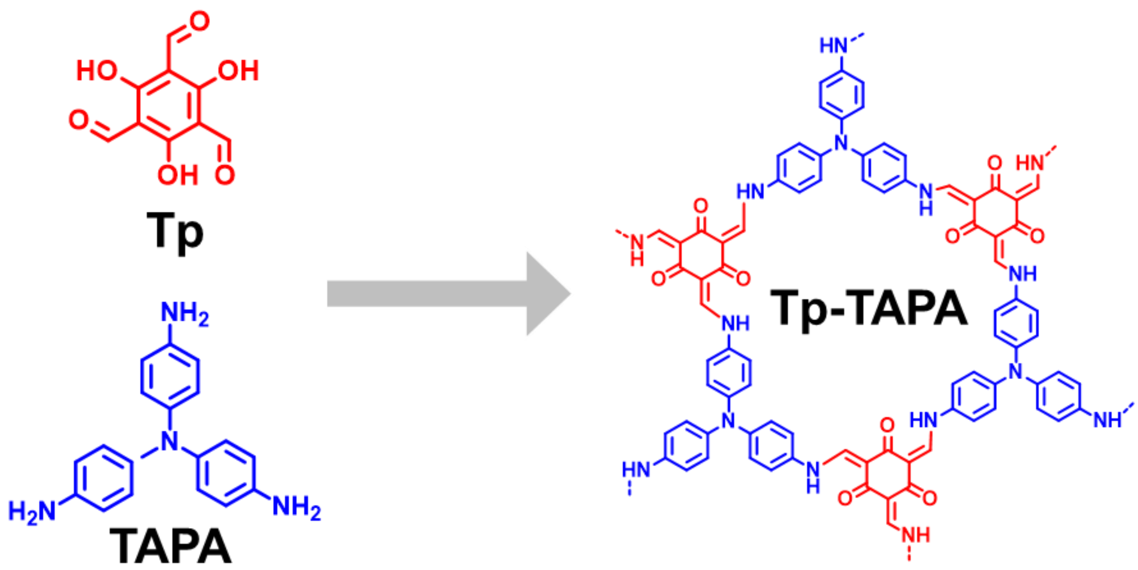

Fig. S34. Reaction for the synthesis of COF Tp-TAPA film.

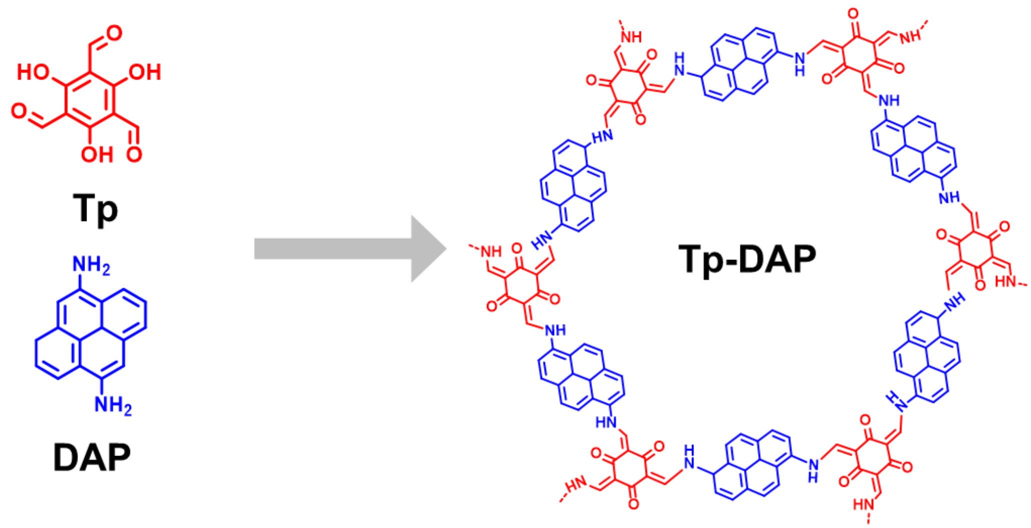

Fig. S35. Reaction for the synthesis of COF Tp-DAP film.

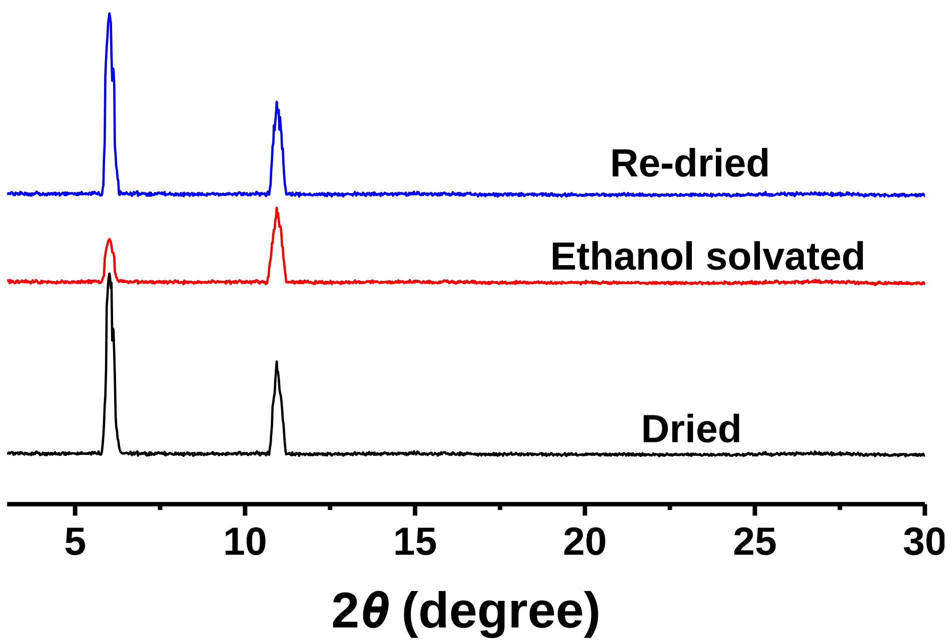

Fig. S36. PXRD patterns of sequential dried−solvated−dried COF Tp-TAPA film in ethanol.

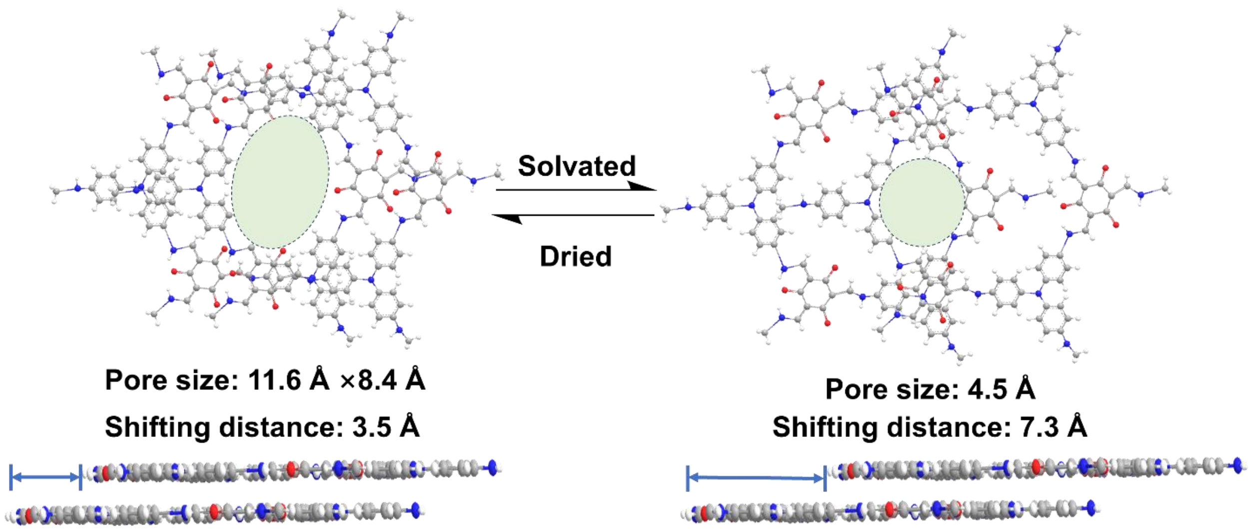

Fig. S37. Simulated structures of COF Tp-TAPA showing reversible transitions between quasi-AB and AB stacking.

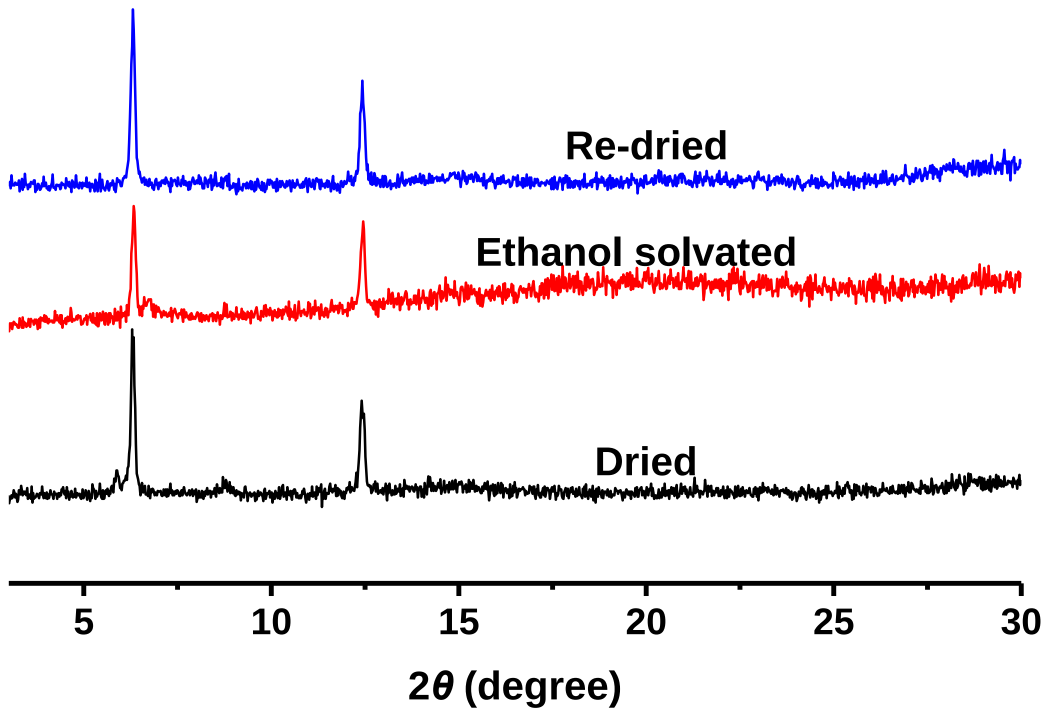

Fig. S38. PXRD patterns of sequential dried−solvated−dried COF Tp-DAP film in ethanol.

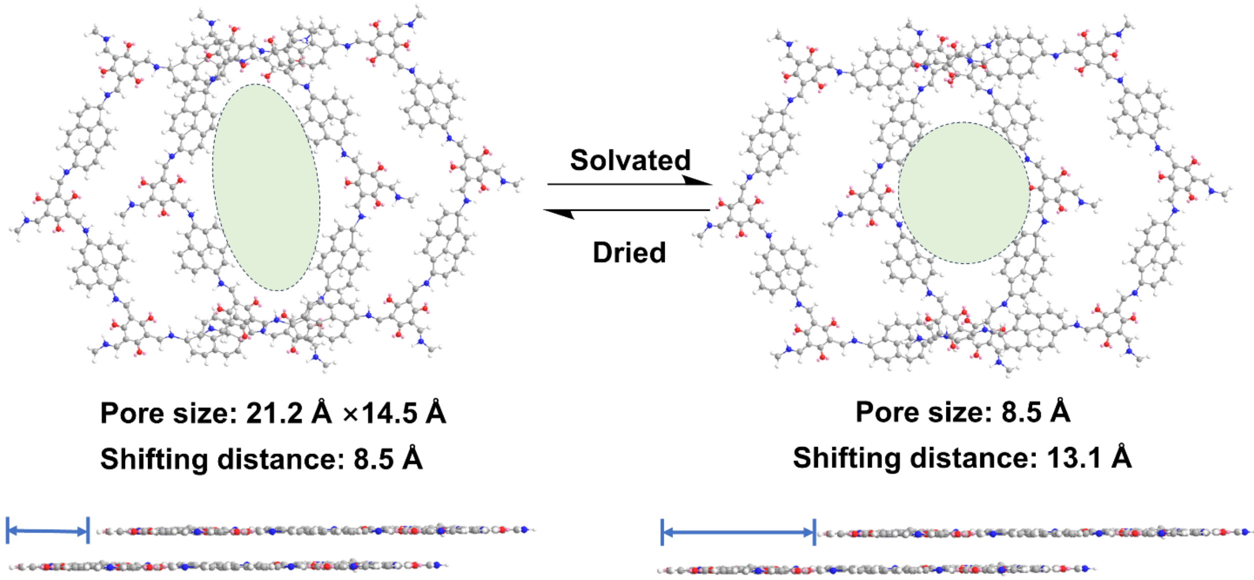

Fig. S39. Simulated structures of COF Tp-DAP showing reversible transitions between quasi-AB and AB stacking.

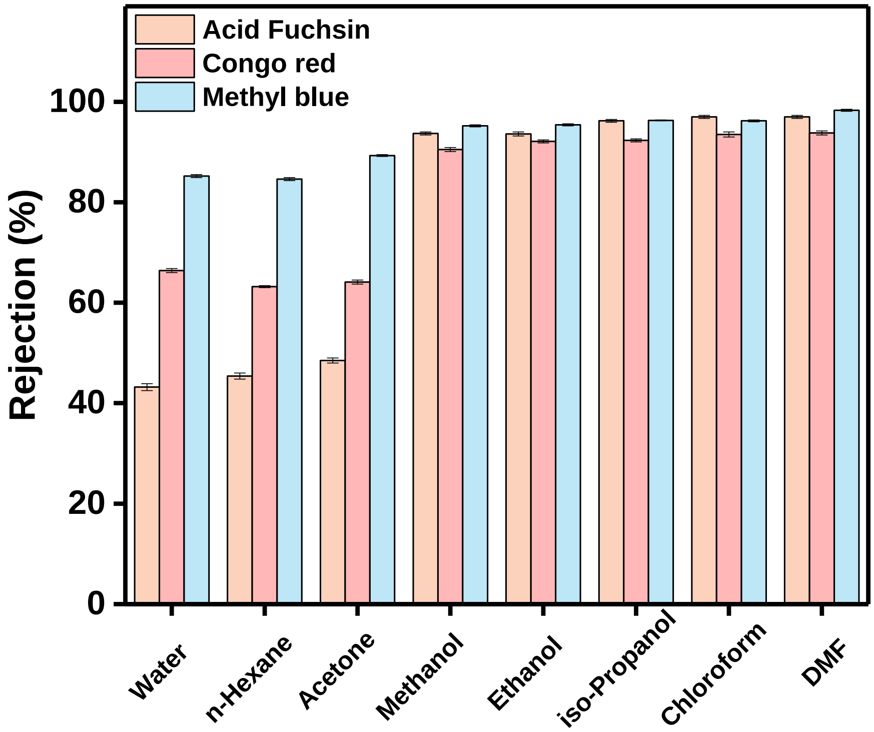

Fig. S40. Dye rejection performance of COF Tp-TAPA membrane in different solvents.

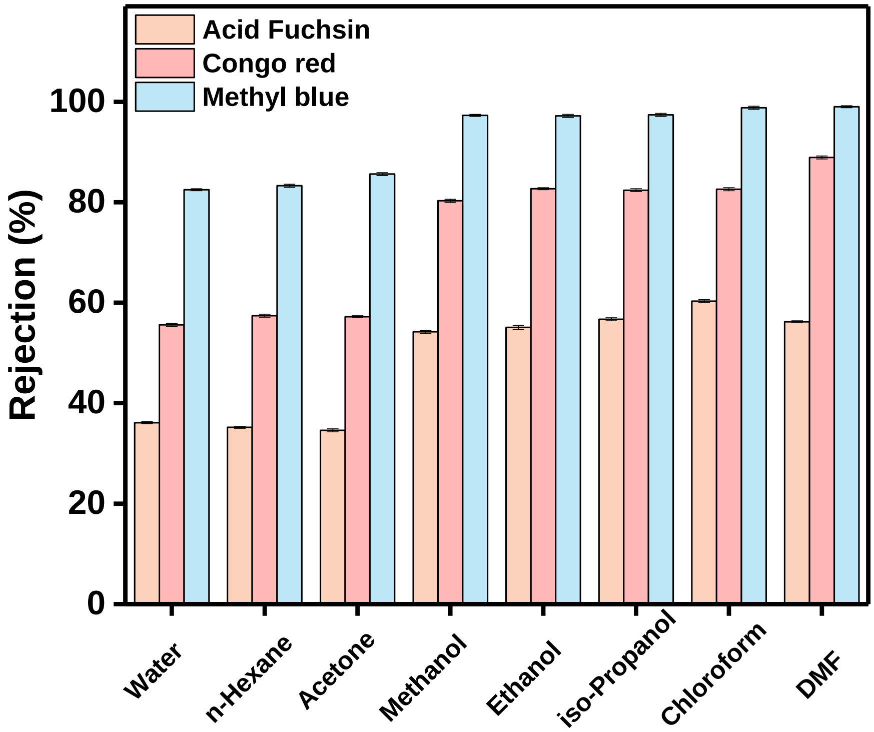

Fig. S41. Dye rejection performance of COF Tp-DAP membrane in different solvents.

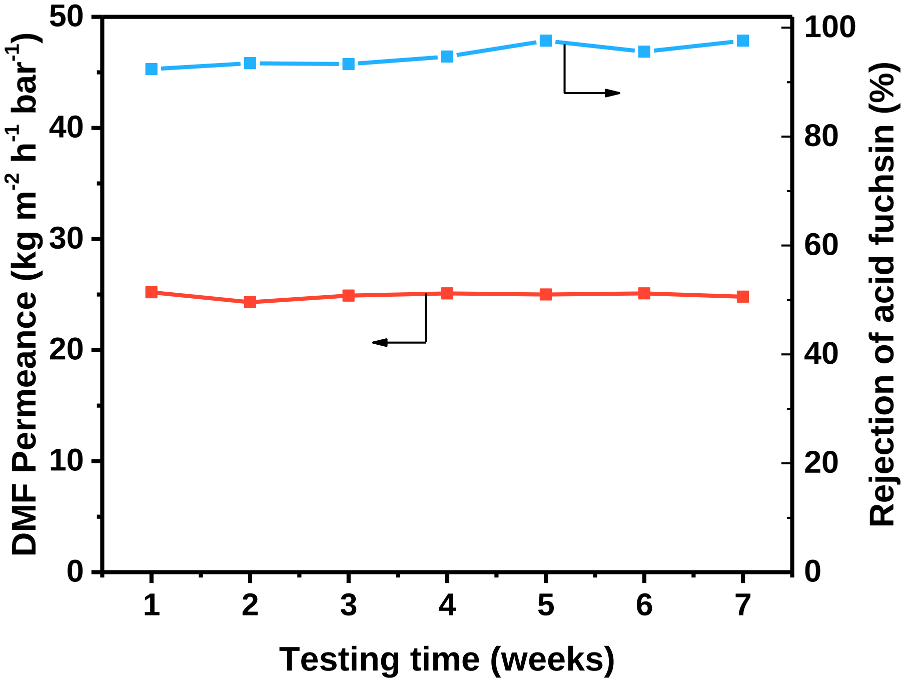

Fig. S42. Long-term stability of COF Tp-TAPA membrane for rejecting acid fuchsin in DMF.

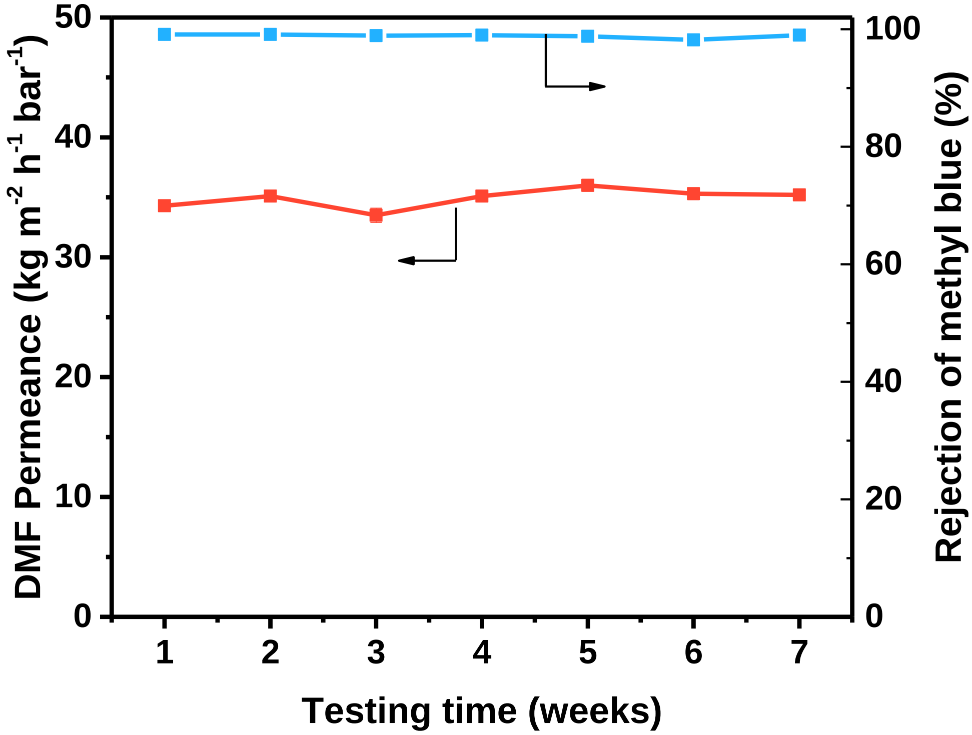

Fig. S43. Long-term stability of COF Tp-DAP membrane for rejecting methyl blue in DMF.

Table S2. OSN performance comparison of state-of-the-art membranes from the literature and this work.

Membrane type	Membrane name	Ethanol permeance (LMH/Bar)	Dye marker (Mw/Da)	Dye rejection (%)	Ref
Microporous polymeric membrane	PTMSP/PAN	4.8	Remazol Brilliant Blue (626)	90	(*27*)
	PIM-1/cellophane	0.1	Remazol Brilliant Blue (626)	98	(*28*)
	PMP/cellophane	0.1	Remazol Brilliant Blue (626)	97	(*28*)
	PTMSP/cellophane	0.2	Remazol Brilliant Blue (626)	95	(*28*)
	PIM-1/PAN	2.9	HPB (535)	78	(*29*)
	MPDTrip-20	2.4	Brilliant Blue R (826)	98	(*30*)
	MPDTMC-20	1.0	Brilliant Blue R (826)	99	(*30*)
	(PIM-1/PEI)/PAN	1.4	HPB (535)	85	(*29*)
	Chloroform vapor annealing-PIM1/PAN	4.3	Tetrazolium blue (727)	92	(*31*)
Dense polymeric membrane	PDMS	4.0	Raffinose (504)	82	(*32*)
	PSF/PEEK	0.7	Rose Bengal (1017)	63	(*33*)
	PEG400/cPI	13.8	Rose Bengal (1017)	83.6	(*34*)
	Cellulose acetate	0.4	Bromothymol Blue (624)	82	(*35*)
	GA-crosslinked PBI	3.7	Brilliant Blue R (826)	99	(*36*)
	DEO-crosslinked PBI	1.0	Remazol Brilliant Blue (626)	99	(*36*)
	$K_2S_2O_8$ crosslinked PBI	2.0	Remazol Brilliant Blue (626)	99	(*37*)
	XDA crosslinked PVDF	2.7	Rose Bengal (1017)	90	(*38*)
	Hydrazine monohydrate crosslinked PAN	2.3	Remazol Brilliant Blue (626)	99	(*39*)
Mixed matrix membrane	CA/gold nanoparticles	1.5	Bromothymol Blue (624)	82	(*35*)
	P84 PI/gold nanoparticles	2.9	Bromothymol Blue (624)	58	(*40*)
	PEBAX/GO	1.9	Brilliant blue (792)	95	(*8*)
	MIL-53 in PMIA	0.7	Brilliant blue G (854)	94	(*41*)
	ZIF-8 in PVDF	4.0	Congo red (696)	94	(*42*)
	PEI-SiO_2/PAN	2.1	PEG (1000)	98	(*43*)
	GNPS-PI	2.9	Bromothymol Blue (624)	58	(*44*)

	POSS + catechol-PI	1.3	Rose Bengal (1017)	99	(*45*)
	MWCNTs-COOHP84	9.6	Rose Bengal (1017)	85	(*46*)
	Annealed MWCNTS-NH_2-P84	2.3	Eosin Y (648)	99	(*47*)
	MWCNTS-NH_2-P84	3.3	Eosin Y (648)	98	(*47*)
GO membrane	rGO-TiO_2/ceramic	4.1	Bromothymol blue (624)	95	(*48*)
	GO-TFN	2.3	Bromothymol blue (624)	89.5	(*48*)
	rGO-TMPyP0.6-44	2.0	Acid fuchsin (586)	92.2	(*49*)
	GO/PI	1.7	Remazol Brilliant Blue (626)	97	(*50*)
	PSS-HPEI-GO/PP	3.1	Rose Bengal (1017)	97	(*51*)
	GO/EDA	1.4	VB12 (1355.4)	85	(*50*)
	0.1GO/2.5 PB	2.4	Rose Bengal (1017)	92.3	(*52*)
	0.2GO/2.5 PB	1.4	Rose Bengal (1017)	98.8	(*52*)
MOF membrane	ZIF-8/PES	8.4	Rose Bengal (1017)	50	(*53*)
	UiO66-NH_2/Matrimid	0.9	Rose Bengal (1017)	96	(*54*)
	PCN-250/ceramic	27.5	Methyl blue (799)	84	(*55*)
COF membrane	Tp-TAPT	15.5	Acid fuchsin (586)	99.6	This work
	Tp-TAPA	25.0	Acid fuchsin (586)	97.6	
	Tp-DAP	35.1	Methyl blue (799)	99.1	

REFERENCES AND NOTES

1. M. Buonomenna, J. Bae, Organic solvent nanofiltration in pharmaceutical industry. *Sep. Purif. Rev.* **44**, 157–182 (2015).

2. P. Marchetti, M. F. J. Solomon, G. Szekely, A. G. Livingston, Molecular separation with organic solvent nanofiltration: A critical review. *Chem. Rev.* **114**, 10735–10806 (2014).

3. R. P. Lively, D. S. Sholl, From water to organics in membrane separations. *Nat. Mater.* **16**, 276–279 (2017).

4. K. Vanherck, G. Koeckelberghs, I. F. J. Vankelecom, Crosslinking polyimides for membrane applications: A review. *Prog. Polym. Sci.* **38**, 874–896 (2013).

5. Z. P. Liao, J. Y. Zhu, X. Li, B. Van der Bruggen, Regulating composition and structure of nanofillers in thin film nanocomposite (TFN) membranes for enhanced separation performance: A critical review. *Sep. Purif. Technol.* **266**, 21 (2021).

6. S. Karan, Z. Jiang, A. G. Livingston, Sub–10 nm polyamide nanofilms with ultrafast solvent transport for molecular separation. *Science* **348**, 1347–1351 (2015).

7. M. H. Abdellah, L. Perez-Manriquez, T. Puspasari, C. A. Scholes, S. E. Kentish, K. V. Peinemann, A catechin/cellulose composite membrane for organic solvent nanofiltration. *J. Membr. Sci.* **567**, 139–145 (2018).

8. J. Aburabie, K. V. Peinemann, Crosslinked poly(ether block amide) composite membranes for organic solvent nanofiltration applications. *J. Membr. Sci.* **523**, 264–272 (2017).

9. C. Li, S. X. Li, L. Lv, B. W. Su, M. Z. Hu, High solvent-resistant and integrally crosslinked polyimide-based composite membranes for organic solvent nanofiltration. *J. Membr. Sci.* **564**, 10–21 (2018).

10. B. Sengupta, Q. B. Dong, R. Khadka, D. K. Behera, R. Z. Yang, J. Liu, J. Jiang, P. Keblinski, G. Belfort, M. Yu, Carbon-doped metal oxide interfacial nanofilms for ultrafast and precise separation of molecules. *Science* **381**, 1098–1104 (2023).

11. G. M. Shi, Y. N. Feng, B. F. Li, H. M. Tham, J. Y. Lai, T. S. Chun, Recent progress of organic solvent nanofiltration membranes. *Prog. Polym. Sci.* **123**, 27 (2021).

12. H. J. Wang, M. D. Wang, X. Liang, J. Q. Yuan, H. Yang, S. Y. Wang, Y. X. Ren, H. Wu, F. S. Pan, Z. Y. Jiang, Organic molecular sieve membranes for chemical separations. *Chem. Soc. Rev.* **50**, 5468–5516 (2021).

13. A. He, Z. W. Jiang, Y. Wu, H. Hussain, J. Rawle, M. E. Briggs, M. A. Little, A. G. Livingston, A. I. Cooper, A smart and responsive crystalline porous organic cage membrane with switchable pore apertures for graded molecular sieving. *Nat. Mater.* **21**, 463–470 (2022).

14. Z. F. Wang, Q. Yu, Y. B. Huang, H. D. An, Y. Zhao, Y. F. Feng, X. Li, X. L. Shi, J. J. Liang, F. S. Pan, P. Cheng, Y. Chen, S. Q. Ma, Z. J. Zhang, PolyCOFs: A new class of freestanding responsive covalent organic framework membranes with high mechanical performance. *ACS Central Sci.* **5**, 1352–1359 (2019).

15. C. S. Diercks, O. M. Yaghi, The atom, the molecule, and the covalent organic framework. *Science* **355**, eaal1585 (2017).

16. U. Diaz, A. Corma, Ordered covalent organic frameworks, COFs and PAFs. From preparation to application. *Coord. Chem. Rev.* **311**, 85–124 (2016).

17. A. P. Cote, A. I. Benin, N. W. Ockwig, M. O'Keeffe, A. J. Matzger, O. M. Yaghi, Porous, crystalline, covalent organic frameworks. *Science* **310**, 1166–1170 (2005).

18. N. Huang, P. Wang, D. L. Jiang, Covalent organic frameworks: A materials platform for structural and functional designs. *Nat. Rev. Mater.* **1**, 16068 (2016).

19. S. Yuan, X. Li, J. Zhu, G. Zhang, P. Van Puyvelde, B. Van der Bruggen, Covalent organic frameworks for membrane separation. *Chem. Soc. Rev.* **48**, 2665–2681 (2019).

20. M. Matsumoto, L. Valentino, G. M. Stiehl, H. B. Balch, A. R. Corcos, F. Wang, D. C. Ralph, B. J. Marinas, W. R. Dichtel, Lewis-acid-catalyzed interfacial polymerization of covalent organic framework films. *Chem* **4**, 308–317 (2018).

21. M. Wang, P. Zhang, X. Liang, J. Zhao, Y. Liu, Y. Cao, H. Wang, Y. Chen, Z. Zhang, F. Pan, Ultrafast seawater desalination with covalent organic framework membranes. *Nat. Sustain.* **5**, 518–526 (2022).

22. C. J. Kang, Z. Q. Zhang, V. Wee, A. K. Usadi, D. C. Calabro, L. S. Baugh, S. Wang, Y. X. Wang, D. Zhao, Interlayer shifting in two-dimensional covalent organic frameworks. *J. Am. Chem. Soc.* **142**, 12995–13002 (2020).

23. L. Wang, J. L. He, M. Heiranian, H. Q. Fan, L. F. Song, Y. Li, M. Elimelech, Water transport in reverse osmosis membranes is governed by pore flow, not a solution-diffusion mechanism. *Sci. Adv.* **9**, eadf8488 (2023).

24. J. L. He, H. Q. Fan, M. Elimelech, Y. Li, Molecular simulations of organic solvent transport in dense polymer membranes: Solution-diffusion or pore-flow mechanism? *J. Membr. Sci.* **708**, 12 (2024).

25. H. Q. Fan, J. L. He, M. Heiranian, W. Y. Pan, Y. Li, M. Elimelech, The physical basis for solvent flow in organic solvent nanofiltration. *Sci. Adv.* **10**, eado4332 (2024).

26. L. Peeva, J. Da Silva Burgal, Z. Heckenast, F. Brazy, F. Cazenave, A. Livingston, Continuous consecutive reactions with inter-reaction solvent exchange by membrane separation. *Angew. Chem. Int. Edit.* **55**, 13576–13579 (2016).

27. A. V. Volkov, V. V. Parashchuk, D. F. Stamatialis, V. S. Khotimsky, V. V. Volkov, M. Wessling, High permeable PTMSP/PAN composite membranes for solvent nanofiltration. *J. Membr. Sci.* **333**, 88–93 (2009).

28. S. Tsarkov, V. Khotimskiy, P. M. Budd, V. Volkov, J. Kukushkina, A. Volkov, Solvent nanofiltration through high permeability glassy polymers: Effect of polymer and solute nature. *J. Membr. Sci.* **423**, 65–72 (2012).

29. D. Fritsch, P. Merten, K. Heinrich, M. Lazar, M. Priske, High performance organic solvent nanofiltration membranes: Development and thorough testing of thin film composite

membranes made of polymers of intrinsic microporosity (PIMs). *J. Membr. Sci.* **401**, 222–231 (2012).

30. Z. Ali, B. S. Ghanem, Y. Wang, F. Pacheco, W. Ogieglo, H. Vovusha, G. Genduso, U. Schwingenschlögl, Y. Han, I. Pinnau, Finely tuned submicroporous thin-film molecular sieve membranes for highly efficient fluid separations. *Adv. Mater.* **32**, e2001132 (2020).

31. J. Li, M. Zhang, W. Feng, L. Zhu, L. Zhang, PIM-1 pore-filled thin film composite membranes for tunable organic solvent nanofiltration. *J. Membr. Sci.* **601**, 117951 (2020).

32. J. Geens, K. Peeters, B. Van der Bruggen, C. Vandecasteele, Polymeric nanofiltration of binary water–alcohol mixtures: Influence of feed composition and membrane properties on permeability and rejection. *J. Membr. Sci.* **255**, 255–264 (2005).

33. Y. Wang, S. H. Goh, T. S. Chung, P. Na, Polyamide-imide/polyetherimide dual-layer hollow fiber membranes for pervaporation dehydration of C1–C4 alcohols. *J. Membr. Sci.* **326**, 222–233 (2009).

34. Z. F. Gao, G. M. Shi, Y. Cui, T.-S. Chung, Organic solvent nanofiltration (OSN) membranes made from plasma grafting of polyethylene glycol on cross-linked polyimide ultrafiltration substrates. *J. Membr. Sci.* **565**, 169–178 (2018).

35. K. Vanherck, S. Hermans, T. Verbiest, I. Vankelecom, Using the photothermal effect to improve membrane separations via localized heating. *J. Mater. Chem.* **21**, 6079–6087 (2011).

36. D. Y. Xing, S. Y. Chan, T.-S. Chung, The ionic liquid [EMIM] OAc as a solvent to fabricate stable polybenzimidazole membranes for organic solvent nanofiltration. *Green Chem.* **16**, 1383–1392 (2014).

37. B. Zhao, G. M. Shi, K. Y. Wang, J.-Y. Lai, T.-S. Chung, Employing a green cross-linking method to fabricate polybenzimidazole (PBI) hollow fiber membranes for organic solvent nanofiltration (OSN). *Sep. Purif. Technol.* **255**, 117702 (2021).

38. M. Mertens, C. Van Goethem, M. Thijs, G. Koeckelberghs, I. F. Vankelecom, Crosslinked PVDF-membranes for solvent resistant nanofiltration. *J. Membr. Sci.* **566**, 223–230 (2018).

39. H. M. Tham, K. Y. Wang, D. Hua, S. Japip, T.-S. Chung, From ultrafiltration to nanofiltration: Hydrazine cross-linked polyacrylonitrile hollow fiber membranes for organic solvent nanofiltration. *J. Membr. Sci.* **542**, 289–299 (2017).

40. K. Vanherck, T. Verbiest, I. Vankelecom, Comparison of two synthesis routes to obtain gold nanoparticles in polyimide. *J. Phys. Chem. C* **116**, 115–125 (2012).

41. L. Zhu, H. Yu, H. Zhang, J. Shen, L. Xue, C. Gao, B. van der Bruggen, Mixed matrix membranes containing MIL-53 (Al) for potential application in organic solvent nanofiltration. *RSC Adv.* **5**, 73068–73076 (2015).

42. Z. Wang, Z. Si, D. Cai, G. Li, S. Li, P. Qin, T. Tan, Improving ZIF-8 stability in the preparation process of polyimide-based organic solvent nanofiltration membrane. *Sep. Purif. Technol.* **227**, 115687 (2019).

43. Y. Li, H. Mao, H. Zhang, G. Yang, R. Ding, J. Wang, Tuning the microstructure and permeation property of thin film nanocomposite membrane by functionalized inorganic nanospheres for solvent resistant nanofiltration. *Sep. Purif. Technol.* **165**, 60–70 (2016).

44. K. Vanherck, I. Vankelecom, T. Verbiest, Improving fluxes of polyimide membranes containing gold nanoparticles by photothermal heating. *J. Membr. Sci.* **373**, 5–13 (2011).

45. Y. C. Xu, Y. P. Tang, L. F. Liu, Z. H. Guo, L. Shao, Nanocomposite organic solvent nanofiltration membranes by a highly-efficient mussel-inspired co-deposition strategy.*J. Membr. Sci.* **526**, 32–42 (2017).

46. M. H. D. A. Farahani, D. Hua, T.-S. Chung, Cross-linked mixed matrix membranes consisting of carboxyl-functionalized multi-walled carbon nanotubes and P84 polyimide for organic solvent nanofiltration (OSN). *Sep. Purif. Technol.* **186**, 243–254 (2017).

47. M. H. D. A. Farahani, D. Hua, T.-S. Chung, Cross-linked mixed matrix membranes (MMMs) consisting of amine-functionalized multi-walled carbon nanotubes and P84 polyimide for organic solvent nanofiltration (OSN) with enhanced flux. *J. Membr. Sci.* **548**, 319–331 (2018).

48. H. Abadikhah, E. N. Kalali, S. Behzadi, S. A. Khan, X. Xu, M. E. Shabestari, S. Agathopoulos, High flux thin film nanocomposite membrane incorporated with functionalized TiO2@ reduced graphene oxide nanohybrids for organic solvent nanofiltration. *Chem. Eng. Sci.* **204**, 99–109 (2019).

49. T. Gao, L. Huang, C. Li, G. Xu, G. Shi, Graphene membranes with tuneable nanochannels by intercalating self-assembled porphyrin molecules for organic solvent nanofiltration. *Carbon* **124**, 263–270 (2017).

50. B. Li, Y. Cui, S. Japip, Z. Thong, T.-S. Chung, Graphene oxide (GO) laminar membranes for concentrating pharmaceuticals and food additives in organic solvents. *Carbon* **130**, 503–514 (2018).

51. D. Hua, T.-S. Chung, Polyelectrolyte functionalized lamellar graphene oxide membranes on polypropylene support for organic solvent nanofiltration. *Carbon* **122**, 604–613 (2017).

52. Y. Gao, K. Su, Z. Li, B. Cheng, Graphene oxide hybrid poly (p-phenylene sulfide) nanofiltration membrane intercalated by bis (triethoxysilyl) ethane. *Chem. Eng. J.* **352**, 10–19 (2018).

53. Y. Li, L. H. Wee, A. Volodin, J. A. Martens, I. F. Vankelecom, Polymer supported ZIF-8 membranes prepared via an interfacial synthesis method. *Chem. Commun.* **51**, 918–920 (2015).

54. D. Ma, G. Han, Z. F. Gao, S. B. Chen, Continuous UiO-66-type metal–organic framework thin film on polymeric support for organic solvent nanofiltration. *ACS Appl. Mater. Interfaces* **11**, 45290–45300 (2019).

55. X. Yu, W. Fan, V. Wee, D. Shi, H. Yuan, Y. Ying, Y. Di Yuan, Z. Yang, Y. Feng, D. Sun, Polycrystalline iron (III) metal-organic framework membranes for organic solvent nanofiltration with high permeance. *J. Membr. Sci.* **644**, 120130 (2022).

56. K. Xu, B. Feng, C. Zhou, A. Huang, Synthesis of highly stable graphene oxide membranes on polydopamine functionalized supports for seawater desalination. *Chem. Eng. Sci.* **146**, 159–165 (2016).

57. B. J. Smith, A. C. Overholts, N. Hwang, W. R. Dichtel, Insight into the crystallization of amorphous imine-linked polymer networks to 2D covalent organic frameworks. *Chem. Commun.* **52**, 3690–3693 (2016).

58. J. Dong, Y. Wang, G. Liu, Y. Cheng, D. Zhao, Isoreticular covalent organic frameworks for hydrocarbon uptake and separation: The important role of monomer planarity. *CrstEngComm* **19**, 4899–4904 (2017).

59. H. Xu, J. Gao, D. Jiang, Stable, crystalline, porous, covalent organic frameworks as a platform for chiral organocatalysts. *Nat. Chem.* **7**, 905–912 (2015).

60. F. Auras, L. Ascherl, A. H. Hakimioun, J. T. Margraf, F. C. Hanusch, S. Reuter, D. Bessinger, M. Döblinger, C. Hettstedt, K. Karaghiosoff, Synchronized offset stacking: A concept for growing large-domain and highly crystalline 2D covalent organic frameworks. *J. Am. Chem. Soc.* **138**, 16703–16710 (2016).

61. L. Nie, C. Y. Chuah, T. H. Bae, J. M. Lee, Graphene-based advanced membrane applications in organic solvent nanofiltration. *Adv. Funct. Mater.* **31**, 2006949 (2021).

62. C. E. Webster, R. S. Drago, M. C. Zerner, Molecular dimensions for adsorptives. *J. Am. Chem. Soc.* **120**, 5509–5516 (1998).

63. A. F. Barton, Solubility parameters. *Chem. Rev.* **75**, 731–753 (1975).